ISOMER ENERGY SOURCE FOR SPACE PROPULSION SYSTEMS

THESIS

Benjamin L. Johnson, Captain, USAF

AFIT/GA/ENY/04-M01

DEPARTMENT OF THE AIR FORCE
AIR UNIVERSITY

AIR FORCE INSTITUTE OF TECHNOLOGY

Wright-Patterson Air Force Base, Ohio

AFIT/GA/ENY/04-M01

ISOMER ENERGY SOURCE FOR SPACE PROPULSION SYSTEMS

THESIS

Presented to the Faculty

Department of Aeronautics and Astronautics

Graduate School of Engineering and Management

Air Force Institute of Technology

Air University

Air Education and Training Command

In Partial Fulfillment of the Requirements for the

Degree of Master of Science in Astronautical Engineering

Benjamin L. Johnson, BS

Captain, USAF

March 2004

AFIT/GA/ENY/04-M01

ISOMER ENERGY SOURCE FOR SPACE PROPULSION SYSTEMS

Benjamin L. Johnson, BS
Captain, USAF

Approved:

/Signed/

Milton E. Franke (Chairman) date

/Signed/

Paul I. King (Member) date

/Signed/

Larry W. Burggraf (Member) date

/Signed/

Maximilian F. Platzer (Member) date

Abstract

Presented in this work are the results of an investigation of alternative means for powering spacecraft and launch vehicles with energy sources other than chemical combustion. Nuclear Thermal Propulsion (NTR) and the energy release of a nuclear spin isomer present potential for increased rocket performance with a compact, high-energy fuel sources replacing the combustion engines of the Delta IV-H 1st and 2nd stage vehicles. NTR was represented by the Nuclear Engine for Rocket Vehicle Application, CERMET, and the Particle Bed Reactor (PBR) fission designs, while the isomer hafnium-178-m2 was investigated in a PBR configuration. Energy storage levels of 1.3 GJ/g are possible with this material, though the successful triggering and maintenance of a chain reaction in this material are still debated topics within the scientific community. The best application for either technology is as an upper stage vehicle with the shielding requirements reduced to that of just a shadow shield between the core and the spacecrafts upper structure. The fission designs are capable of specific impulse values between 800 and 1,000 s leading to mass savings in the range of 7,000 to nearly 10,000 kg once the engine masses and shielding have been included. An isomer core in the configuration of a 19-element PBR may be able to achieve a specific impulse on the order of 880 s with the isomer in metallic form, and specific impulse values as high as 1,090 s if the isomer is in the form of hafnium carbide. This translates to somewhere between a 5,000 and 9,000 kg depending on the material makeup of the core and heat efficiency. Payload mass increases by a factor of two or greater velocity change capability are the payoffs of these systems.

In loving memory of Joanne Johnson, 12/17/1949 to 8/27/2003

Acknowledgments

I would like to thank my advisor Dr. Milton Franke, the readers on my thesis committee; Dr. Burggraf, Dr. King, and Dr. Platzer, and my professors at AFIT for providing me with the tools needed to undertake this effort spanning a wide spectrum of scientific and engineering fields. Dr. Burggraf was especially helpful in providing last minute direction on some very important issues. I'd also like to thanks my sponsors from AFRL/PRAS for allowing me to work a research topic that I had great personnel interest in. Being a part of the '04 class at AFIT was a benefit to my development and I thank my classmates and hope to work with many of them again in the near future.

Benjamin L. Johnson

Table of Contents

Page

Page

List of Figures

List of Tables

Page

Nomenclature

Symbol	Description
a	Acoustic velocity (m/s)
al	Orbital altitude include Earth radius (km)
A	Pellet surface area (m^2)
α	Alpha particle (^4_2He)
$B(\mu,x)$	Buildup factor
$B_a(\mu,x)$	Buildup factor for energy absorption
β	Beta particle (^-e)
c	Speed of light (2.9979×10^8 m/s)
c_p	Specific heat capacity (kJ/kmol-K)
cr	Consumption rate measured in mass of hafnium isomer (kg/s)
c^*	Characteristic velocity (m/s)
CE	Gamma-radiation energy release (W)
$\dot{D}$	Dose rate (rad/s)
$\dot{D}_o$	Allowable dose at a distance r (rad/s)
Δ	Change in values from initial point to final point
E	Energy of a particle or photon (keV)
Eff	Efficiency of energy absorption for point source gamma emitter
E_o	Photon energy (MeV)
ε	Expansion ratio
f	fractional enhancement in decay rate
f_{inert}	Inert mass fraction
F	Thrust (N)
g	Average fraction of kinetic energy emitted as bremsstrahlung
g_o	Gravitational constant (9.81 m/s^2)
γ	Ratio of specific heats
h	Planck's constant ($6.6260755 \times 10^{-34}$ J-s)
h_u	Enthalpy of vaporization at 300 K (kJ/kmol)
$H(R,x)$	Energy absorbed in a material (W/cm^3)
H_{core}	Core height (cm)
I	Radiation intensity (photons/cm^2)
I_{sp}	Specific impulse (s)
k	Thermal conductivity (W/m-K)
λ	Wavelength (m)
m	Mass (kg)
m_{extra}	Mass savings (kg)
m_i	Initial rocket vehicle mass (kg)
m_f	Final rocket vehicle mass (kg)
m_{Hf}	Mass of hafnium isomer to supply minimum mission power (kg)

Symbol	Description
m_l	Payload mass (kg)
m_p	Propellant mass (kg)
m_{pellet}	Mass of an individual pellet (kg)
m_{prop}	Mass of propellant carried on liquid rocket versions (kg)
m_{pv}	Pressure vessel mass (kg)
m_s	Structural mass (kg)
$\dot{m}$	Mass flow rate (kg/s)
μ	Linear attenuation coefficient (cm^{-1})
μ_e	Gravitational Parameter ($3.896004(10)^5$ km^3/s^2)
μ_A	Linear energy-absorption coefficient (cm^{-1})
μ_{tr}	Linear transmission coefficient (cm^{-1})
μx	Relaxation length
μ / ρ	Mass attenuation coefficient (cm^2/g)
μ_A / ρ	Mass energy-absorption coefficient (cm^2/g)
μ_{tr} / ρ	Mass energy-transfer coefficient (cm^2/g)
M	Mach number
M_1	Mach number at core inlet
M_2	Mach number at core outlet
M_3	Mach number at nozzle exit
MM	Molar mass (kg/kmol)
MWt	Thermal megawatt
N_d	Number density (pellets/m^3)
N_p	Number of pellets
ν	Photon frequency (Hz)
f_{pv}	Pressure vessel mass factor (m)
Φ	Irradiating photon flux (photons/s-keV-cm^2)
P	Pressure (Pa)
P_c	Chamber pressure (Pa)
P_e	Pressure at nozzle exit (Pa)
P_o	Stagnation pressure (At core outlet used as chamber pressure) (Pa)
P_{bvm}	Percent by volume of the core that is moderator
P_{bvp}	Percent by volume of the core that is pellets
P_{core}	Core power (W)
P_{den}	Power density of core (W/m^3)
P_{drop}	Percentage value of pressure drop through core
P_{rad}	Radiated power (W)
P_{req}	Required core power (W)
q_{max}	Maximum energy added to fluid before thermal choking occurs (J/kg)
Q	Quality factor

Symbol	Description
$\dot{Q}_x$	Power (W)
r	Density (g/cm^3)
r_{core}	Core density (kg/m^3)
rad	Unit of absorbed dose (1 rad = absorption of 100 erg/g)
rem	Unit of equivalent dose (rem = Q x rad)
R	Radius of sphere surrounding point source (cm)
R_{core}	Core Radius (cm)
Ru	Universal gas constant (8.314 kJ/kmol-K)
s_{int}	Integrated cross section (cm^2-keV)
s	Seconds
S	Source strength (photons/s)
S_l	Shield loading factor (kg/m^2)
t	Lifetime of isomeric state (s)
$\Gamma^o(R,x)$	Current density of uncollided photons (photon/cm^2-s)
t_b	Burn time (s)
T	Static temperature (K)
T_o	Stagnation temperature (K)
T_o / T_o^*	Tabulated ratio at given Mach number
v	Velocity (m/s)
v_e	Exhaust velocity (m/s)
V	Volume (m^3)
V_{core}	Core volume (m^3)
V_{pi}	Interior volume of individual pellet (m^3)
V_{po}	Entire volume of individual pellet (m^3)
V_{pv}	Pressure vessel volume (m^3)
x	Material thickness (m)
$^{178}Hf^{m2}$	Isomeric form of hafnium
AEC	Atomic Energy Commission
AFOSR	Air Force Office of Scientific Research
CERMET	Matrix of metals
DARPA	Defense Advanced Research Projects Agency
DOE	Department of Energy
EOARD	European Office of Aerospace Research and Development
HALE	High Altitude Long Endurance
ICBM	Intercontinental Ballistic Missile
LET	Linear Energy Transfer
NASA	National Air and Space Administration
NEET	Nuclear Excitation by Energy Transfer
NERVA	Nuclear Engine for Rocket Vehicle Application

Symbol	Description
NIST	National Institute of Standards and Technology
NRX	Nuclear Reactor Experiment
NTR	Nuclear Thermal Rocket
PBR	Particle-Bed Reactor
SNTP	Space Nuclear Thermal Propulsion
TIC	Triggered Isomer Core
TIHE	Triggered Isomer Heat Exchanger
UAV	Unmanned Aerial Vehicle
U.S.	United States

ISOMER ENERGY SOURCE FOR SPACE PROPULSION SYSTEMS

I. Introduction

1.1. Motivation

The current capabilities of our space propulsions systems are limiting human operation within and about the space environment. Chemical rocket systems, while necessary for launch operations due to their high thrust characteristics, do not achieve the highest levels of fuel economy. This economy is measured by a vehicle's specific impulse (I_{sp}) value which represents the time a rocket can produce one pound of thrust using one pound of fuel. Further complexities within a rocket design are introduced with the choice of relying on chemical propulsion; since both a fuel and oxidizer are required, must be stored separately, and be fed to the combustion chamber. Near earth propulsion systems relying on solar power, while efficient in terms of fuel economy (solar thermal) or requiring no fuel at all (solar-lightsail), lack the thrust required for rapid acceleration and short time-scale missions. The inability of chemical and solar powered spacecraft to both "rapidly and efficiently" operate in the space environment is delaying mankind's progress in its quest to explore, utilize space assets to better life on Earth, and expand our civilization in such a manner that it allows us to grow as a nation and world community. The new challenges presented by life in space will lead to new ideas, new technologies,

and ultimately to an evolution of our society. While there will always be those among us content with living in a society that does not extend its reach into space, many people now realize the importance of space and the benefits that conquering this domain will have on our way of life (1). Settling this new frontier, or establishing a permanent presence in space is important, and it is rapidly being realized that the use of energy sources other than chemical or solar are needed to make this vision a reality.

While it is possible to operate near-earth with chemical or solar powered systems, the key to human advancement is efficient and rapid transport reducing the timescales of operations in the space environment. What is required is an alternative fuel source high in energy density and capable of releasing this energy on demand. For the past sixty years scientists and engineers have contemplated, researched, engineered, designed, tested, and even flown a few systems powered by nuclear fission or radioactive decay (2:10-15; 3:452-459; 4:12-19; 5; 6). These vehicles ranged from launch systems to deep space probes and spacecraft.

Deep space missions are most often discussed as the target for space nuclear reactors; this is more an area of interest for the National Air and Space Administration (NASA) (7) than for the Air Force, and not the only need for such propulsion sources. Near term there is a need for increasing payload amounts delivered to space and for missions reaching out as far as the moon (8), therefore; an investigation of nuclear electric propulsion was not included in this study.

While concepts like controlled nuclear fusion and antimatter systems are still in the far-off future, fission reactors (well understood and operated for terrestrial energy generation and naval vessel propulsion) would appear to be the near-term solution to the

problem. However, many hazards are associated with the production, storage, handling, and use of fission reactors, which is why today we are still relying on chemical systems. If the hazards of fission reactors cannot be overcome or accepted, another source of energy is required to satisfy this need. It is possible to achieve metastable excited energy states in some nuclei which can serve as a means of energy storage. Nuclear spin isomers, in particular, the isomer hafnium-178-m2 ($^{178}Hf^{m2}$) stores approximately 2.446 MeV per atom or 1.3 GJ/g with a 31-year half-life (9). Research and experiments conducted over the past 5 years have indicated that it may be possible to trigger this isomer to release its stored energy on demand (10:4). This is indeed remarkable since gram quantities can store energies equivalent to metric ton quantities of chemical fuels or explosives (10:4). In addition, the spectrum of ionizing radiation released by this decay is different from that seen in a conventional fission reaction. Nuclear fission results in the production of fission fragments, neutrons, alpha and beta particles, and gamma-rays. Gamma-rays, in particular, can range from 0.2 to 7.6 MeV in energy, from the fission of U^{235} (11:7-72). With the decay of $^{178}Hf^{m2}$ the energy released is entirely in the form of gamma-rays ranging from 12.7 to 547 keV. If this released energy could be used to heat a propellant (directly or indirectly) to significant temperatures then there is potential for a new source of energy to transport us rapidly through the space environment.

1.2. Research Objective

The goal of this research was to determine how triggered isomer decay could best be utilized as a source of heat energy in a nuclear thermal rocket (NTR) configuration. This includes study of the current state of triggered isomer research, an investigation of

the interaction of isomer decay products with materials, research into the best suited nuclear reactor design, and comparisons against chemical and nuclear propulsion systems as they are used in fielded systems today or proposed to be used in the systems of tomorrow.

The successful triggering of the isomer $^{178}Hf^{m2}$ is a highly-debated topic. To date only a few experiments have demonstrated successful triggering of this material, and these have not been universally accepted by the scientific community (12; 13; 14; 15; 16; 17). The belief that triggering is possible is necessary for this research, but a summary of the research conducted by scientists on both side of the debate is included in Sec. 2.1 of this document to accurately represent the maturity of triggered isomer technology.

All debates about the triggering of $^{178}Hf^{m2}$ aside, the primary concern becomes absorbing the electromagnetic radiation released by the radionuclide decay. The attenuation, and energy deposited by this gamma radiation becomes important when one tries to heat a propellant or shield a spacecraft and its surroundings from radiation given off by the core.

The most heavily researched thermal reactors designed for space use are the Nuclear Engine for Rocket Vehicle Application (NERVA), the Particle Bed Reactor (PBR), and the CERMET reactor (3:452-459; 4:12-19; 5; 6; 18; 19; 20; 21). While none of these reactors ever made it to production, enough testing was conducted to prove the concepts, especially in the case of the NERVA rocket which made it all the way to full-scale testing. Table 1 lists the capabilities of these reactors as they were designed. Each reactor design is unique in its operating principal but this study will aim at determining

the traits of each reactor design that would be most beneficial to a triggered isomer design.

Table 1. Comparison of Possible Near-Term Concepts for Reactors (3:457)

Nuclear Engine	NERVA	CERMET	PARTICLE-BED
Power (MW)	1,570	2,000	1,945
Thrust (N)	334,061	445,267	333,617
Propellant	H_2	H_2	H_2
Fuel Element	Solid rod	Solid rod	Porous particle bed
Maximum Propellant Temperature (K)	2,361	2,507	3,200
Isp (s)	825	930	971
$\dot{m}$ **(kg/s)**	41.27	48.81	35.02
Chamber Pressure (MPa)	3.102	4.136	6.176
Nozzle Expansion Ratio	100	120	125
Engine Mass (kg)	10,138	9,091	1,705
Total Shield Mass (kg)	1,590	1,590	1,590
Engine *F/W* (no shield)	3.4	5.0	20.0

A similar core design replacing the fission fuel with the isomer $^{178}Hf^{m2}$ is the starting point for this work. This will have to be carried out in such a manner that a chain reaction is ignitable and maintainable, though it is realized at this time that scientists and engineers may be a long way from achieving this experimentally. In essence, the best reactor design to support triggered isomer decay will be identified through an analysis of materials and geometry. This will be followed by a comparison against the baseline

fission reactor and then comparisons against chemical systems used in the selected mission to see if there is a potential for performance improvements.

The vehicle that was examined in this study was the Delta IV-Heavy launch vehicle, both its 1st and 2nd stages. The Delta IV-H rocket was chosen because it is one of the most powerful rockets that will be used to boost payloads into orbit in the next few years. It also already incorporates cryogenically-fueled stages that hopefully will eliminate the need for drastic alterations to the propellant storage and handling system with an alternative design. Table 2 lists the performance characteristics of each of these stages.

Table 2. Vehicle Design Parameters (22)

Vehicle Name	1st Stage Delta IV-H	2nd Stage Delta IV-H
Inert Mass (kg)	80,280	3,490
Propellant Mass (kg)	598,800	27,200
Vacuum Thrust (N)	9,945,000 {3 engines}	110,000 {1 engine}
Chamber Pressure (MPa)	9.72	3.21
Vacuum Isp (s)	420.0	462.4
Nozzle Expansion Ratio	21.5:1	285:1
Propellant Mass Fraction	0.88	0.89
Vehicle *F/W* (with 10,843 kg payload)	1.4	0.27
Δv (km/s)	7.84*	4.62*

The thrust values shown are average vacuum thrust levels and the number in brackets indicate the combined number of engines producing this thrust. The velocity values (asterisked) were calculated based on specific mission goals and these calculations are

displayed in Appendix F. In the case of the Delta IV-H 1st stage the velocity change (Δv) calculated was that velocity needed to enter a circular orbit at an altitude of 110 km above the Earth. The 2nd stage velocity change was determined from knowledge of the 2nd stage specific impulse, burn time, vehicle mass, and thrust value assuming constant thrust. This allowed for determining the mass flow rate, propellant exhaust velocity, and finally its Δv through use of the ideal rocket equation shown in Eq. [23]. Once a reactor design is identified that has the highest potential for successfully operating on the principals of triggered isomer decay, the performance will be compared against what is predicted for the current design which is combustion driven.

1.3. Past Work.

Prior to this research effort two other studies, both by master's students at the Air Force Institute of Technology, focused on propulsion applications for using triggered isomer energy. The first study was conducted by Captain Carl Hartsfield, and was entitled "Analysis of the Application of a Triggered Isomer Heat Exchanger as a Replacement for the Combustion Chamber in an Off-the-Shelf Turbojet" (23), completed in March 2001. Hartsfield modeled variations of flat plate configuration, solid-state heat exchangers with the commercial software package, ANSYS® 5.6.1 (24). Three basic heat exchanger geometries were studied, and Hartsfield concluded that all could produce sufficient heat transfer to replace the combustion chamber in the J-57 turbojet engine used in the Boeing 707, KC-135, and B-52 (23:XV). In this design the heat exchanger was assumed to be manufactured from the isomer material and heater exit temperatures resulted in the range of 986 to 1,150 K with sea-level thrust values from 37,000 to 47,000

N. Though constant heat generation is likely the most accurate model of the isomer decay process, it was deemed too computationally complex and a constant surface temperature of 2,400 K was applied to all the surfaces of the heat exchanger. This decision between modeling with constant surface temperature and constant surface heat flux was made on the basis of the temperature gradient for the constant surface temperature condition most nearly matching that of the constant heat generation condition. All of the radiation escaping the engine was assumed to be in the form of 600 keV gamma-rays, which is slightly higher than the most energetic photon emitted during the natural decay of $^{178}Hf^{m2}$ which is 574 keV (25). Only 5% of the heat generated in the decay process was assumed to escape the heat exchanger by radiation to the surroundings. Stagnation temperatures, pressure losses, radiation shielding, and the physical dimension of a triggered isomer heat exchanger were all examined in this study with the result being a predicted heat exchanger volume of 0.042 m^3 and weight of approximately 420 kg.

Captain Chris Hamilton followed up this work with a "Design Study of Triggered Isomer Heat Exchanger-Combustion Hybrid Jet Engine for High Altitude Flight" (2), in March 2002. A Global Hawk Unmanned Aerial Vehicle (UAV) relying on a conventional combustion engine for takeoff and near-earth operation, and a triggered isomer heat source for high altitude flight (>20,000 ft) was the subject of this study. It was concluded in this work that a single hybrid engine with a switchover from conventional combustion to Triggered Isomer Heat Exchanger (TIHE) operation could extend the endurance of a High Altitude Long Endurance Aircraft (HALE) weeks beyond the current mission limitation which was on the order of days (2). Up to a 20% drop in

vehicle weight was also possible primarily due to lower fuel requirements (2). Weight estimates including 8.9 kN for the triggering photon source and engine modifications, 11.6 kN for semispherical shielding, and 6.67 kN for the TIHE, were also made (2). Hamilton used Aircraft Engine Design System Analysis Software (AEDsys), version 2.13 (26) and On-Design Analysis of Gas Turbine Engines (ONX), version 4.021 (27) for basic engine design and performance analysis. The same assumptions from Hartsfield's study concerning the heat exchanger design were carried over into this study with the addition of the requirement that the heat exchanger produce equal heating rates to the chemical combustors it was replacing. The development of a specific reactor design and its method of manufacture were left as areas for further investigation by both studies. No other studies of using a triggered isomer energy source for propulsion were found in the literature search performed.

2. Background/History

2.1. Triggered Isomer Development

The 4-quasiparticle isomer of hafnium with excitation energy equal to 2.446 MeV and a 31-yr half-life (9) represents a compact, long duration means of energy storage that recent experiments (9; 10; 28; 29; 30:2-3) have shown can be manipulated to release its energy on demand. Some shell-model calculations have also suggested the existence of more extreme isomers such as the neutron-rich hafnium isotopes, and in the isotopes of lutetium (Z = 71) and tantalum (Z = 73) (31:84-85), but the amount of research put into the study of the hafnium isomer to date makes it the most likely candidate for actual applications. The term nuclear isomer is used to describe long-lived, high-energy states of excitation in nuclei, as opposed to the term chemical isomer which describes a variation in the bond arrangement of a molecule. The hafnium nuclear isomer can be formed by bombarding tantalum with protons in a process that requires a nuclear reactor or particle accelerator. Quantities of this isomer are also produced in Dubna, Russia by bombarding ^{176}Yb with alpha-particles. Bombardment of these materials results in decay to the $^{178}Hf^{m2}$ isomer, in the instance where energy is transferred to the excited states of product nuclei instead of manifesting as kinetic energy of escaping products. At present only small quantities of the isomer can be produced and are available for experimentation. SRS Technologies in Huntsville, Alabama, is under contract with the Air Force Research Laboratory for a supply of the isomer, but at present only a ten-thousandth of a gram quantity can be generated at a given time and the cost of production

is likely to be expensive (32). A near-term goal for production of the isomer would be on the order of 100 grams per year (25), and with 1.3 GJ stored per gram this equates to 130 GJ stored per year.

In the case of most isomers the energy absorbed during formation is reradiated, but in rare situations, such as with this hafnium isomer, "large differences between the spins of the isomeric and ground states, (and) differences between their projections on the symmetry axis (K quantum number)" (33:167) inhibit this decay. In the case of $^{178}Hf^{m2}$, the spontaneous decay is restricted for decades. The challenge then is to get the isomer to release its stored energy on demand; a feat that some scientists are now convinced is achievable.

The Air Force Office of Scientific Research (AFOSR), Defense Advanced Research Projects Agency (DARPA), Department of Energy (DOE), and the European Office of Aerospace Research and Development (EOARD) have all been primary sources of funding for research of the triggering and development of this very special isomer and a few others. In 1999, under AFOSR sponsorship, an article entitled "Accelerated Emission of Gamma Rays from the 31-yr Isomer of $^{178}Hf^{m2}$ Induced by X-Ray Irradiation," was published in the Physics Review Letters by C.B. Collins *et al.* (9) from the University of Texas at Dallas. In the experiments conducted at the university, a dental x-ray machine set to endpoint energies of 70 and 90 keV was used to irradiate samples of $^{178}Hf^{m2}$ with the hopes of triggering the release of the total energy stored within the nucleus of the isomer. A dental x-ray machine produces bremsstrahlung radiation; which is a continuous spectrum of x-ray photons generated due to the deceleration of charged particles. In this case electrons were the charged particles being

decelerated and the x-ray machine was operated at 15 mA. Photon intensities on the order of 10^{10} photons/keV-s (9) were produced on the 1 cm diameter target containing 6.3 x 10^{14} isomeric nuclei. The consortium (9; 10; 28; 29) reported $4 \pm 2\%$ increases in the intensity of the 495 keV emission line emitted during spontaneous decay due to irradiation with photons below 90 keV in energy. The range of interest for incident photon energies was shortly after identified to be between 20 and 60 keV. This paper recommended that further research be conducted to obtain better measurements of the energy required to trigger the decay of the isomer, and subsequent experiments have since tried to better identify this requirement as well as improve the measurement techniques that are used to identify successful triggering of the isomer.

The release of this initial report, however, sparked a hot debate within the scientific community partially because the size of the cross section for photon interaction reported was much larger than allowed according to theory, and the $4 \pm 2\%$ increases in spectral intensity were not large enough to convince many that they were witnessing a successful triggering event (15). The reported integrated cross section (s_{int}) for the triggering was 10^{-21} cm^2-keV, which some scientists claim is beyond the realm of physical possibility (13). The integrated cross section can be calculated by multiplying the cross section for photon interaction by the reaction branch energy width that excites the isomer to the desired K-mixing level resulting in decay past the isomeric to the ground state (10). In turn, this integrated cross section is related to the fractional enhancement of the decay rate (f), the irradiating photon flux (Φ), and the lifetime of the isomeric state (t =1.4 x 10^9 s) as shown in Eq. [1].

$$s_{int} = \frac{f}{\Phi t} \qquad [1]$$

Under DOE sponsorship a consortium from Lawrence Livermore, Los Alamos, and Argonne National Laboratories conducted an experiment in attempt to verify Collins results (14). An Advanced Photon Source (APS) was used, and the paper released in 2001 (17) reported that no accelerated emission was observed. The APS used produced a "white" beam of incident radiation with intensities ranging from 10^{11} to 10^{15} photons/keV-s across the 20 to 60 keV region of interest. In this first experiment the team at Argonne, with photon of energy between 20 to 60 keV incident on 0.03 cm^2 targets containing 7.3 x 10^{14}, 3.0 x 10^{15}, and 6.4 x 10^{15} isomeric nuclei, calculated a cross section for triggering that was below 2 x 10^{-27} cm^2-keV. This was many orders below the 10^{-21} cm^2-keV results achieved in the Texas experiments, and these researchers claimed that the results witnessed were consistent with what is predicted by nuclear physics using an experimental setup that was orders of magnitude more sensitive than the initial Texas experiments (14).

The consortium lead by Collins, however, still had confidence in the results of their past experiment and followed it up with further experiments using a monochromatic photon source (Spring-8 in Japan). This type of source is capable of producing a narrow-band of incident x-rays on a target, as the energy bandwidth is only 0.5 eV wide. The results of this testing indicated, once again, successful triggering of the $^{178}Hf^{m2}$ and served as a verification of the results obtained in earlier testing. In Collins summary of the work accomplished to date in 2001 (10), he reported a 4 keV (9 to 13 keV) bandwidth for the absorption of trigger photons and a cross section not much reduced from the 10^{-21}

cm^2-keV value obtained earlier, showing promise of a self-sustained reaction within a material after the initial triggering event. In addition to this, a new gamma-ray line of 129.4 keV was detected coincident with the ground state band 213.4 keV transition, signifying a recognizable affect of photon irradiation. A second experiment by the team at Argonne with the intent of studying incident energies below 20 keV did not detect this new line and produced a slightly larger cross section 10^{-26} cm^2-keV than previous experiments, but still yielded no evidence of successful triggering (12).

The scientific methods utilized by the researchers in these studies will not be examined in this work, but the work done by Collins et. al. (9; 10; 28; 29) will be a basis for moving on and addressing issues with the application of this technology. Collins has gone further in stating that the ionization of L-shell electrons of $^{178}Hf^{m2}$ has a 0.2% chance of triggering the release of the energy stored in the nucleus (10), and linked triggered decay of $^{178}Hf^{m2}$ with the Nuclear Excitation by Energy Transfer (NEET) process. This process begins with the photoionization event, and when the vacancy is filled by the transition of an electron from a higher orbital shell, energy is transferred to the nucleus instead of to an emitted photon. The benefit of relating this process to triggering is that the cross section is increased due to the incident photon being able to interact with the entire atom instead of just the nucleus to initiate decay. Collins reports a photoionization cross section at the L_1 edge of 7.5 x 10^{-20} cm^2 and links 90% of the triggering events to x-ray energies corresponding to the L-shell edges for photoionization of the electrons of $^{178}Hf^{m2}$ (10). Investigation of the actual mechanism by which the decay process proceeds will be avoided in this study, and the assumption that incident x-rays can trigger the release of the stored energy in $^{178}Hf^{m2}$ will be made. The diagram

below shows the natural decay process beginning with the emission of either a 12.7 keV or 309.5 keV photon. The actual ranges of trigger photon energy still under investigation are from 9 to 12 keV, ~40 keV, and ~60 keV (34).

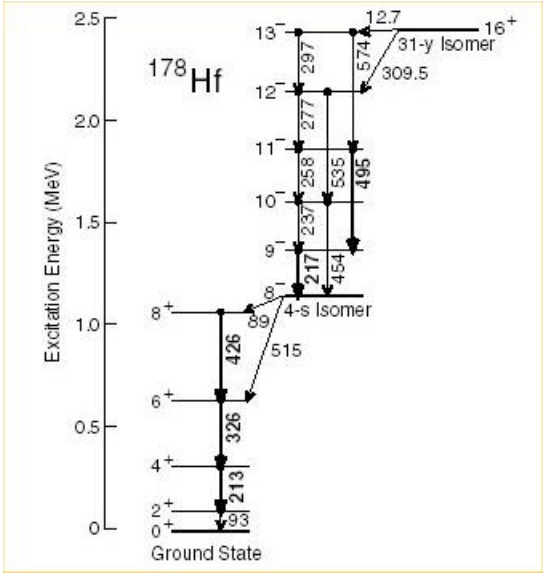

Figure 1. Energy Level Diagram of $^{178}Hf^{m2}$ Decay (13)

Experiments funded by AFOSR and DARPA are ongoing at the University of Texas at Dallas and Youngstown State, with aims at gaining a better understanding yet of the stimulated decay, and work under EOARD sponsorship is continuing internationally (35). DARPA is also financing the production of this isomer at several industrial firms.

2.2. **Radioactive Decay.**

2.2.1. **Forms of Radioactive Decay.**

There is a significant difference between the decay products generated by $^{178}Hf^{m2}$ and those generated by conventional fission reactors. Fission is a process where a heavy nucleus is split by a fast moving neutron resulting in the formation of new nuclei, neutrons, electromagnetic radiation, electrons,

and massless uncharged particles called antineutrinos. The particles that are released are moving very fast and their high kinetic energy values are the result of the release of nuclear binding energy. Once these particles interact and collide with other atoms in the fuel material, reactor core, or coolant, their energy can be transferred to thermal energy. The recoverable energy from a fission reaction is approximately 200 MeV per nucleus which is available in the form of heat. This energy is distributed among the fission fragments and particles as displayed in Table 3.

Table 3. Representative Distribution of Fission Energy (3:471)

Energy Source	**Fission Energy (MeV)**
Fission fragments	168
Neutrons	5
Prompt gamma-rays	7
Delayed radiation Beta particles Gamma-rays Radiative capture gammas	 8 7 5
Total	200

As a comparison only 2.446 MeV is given off from $^{178}Hf^{m2}$ as prompt gamma-rays during decay, necessitating many times the number energy producing events taking place, when compared against fission, if the energy available to heat the propellant is to be similar.

Forms of radiation usually have associated with them a Linear Energy Transfer (LET) value which is related to the level of interaction that radioactive particles have with the medium they are passing through. Neutrons and alpha (α)-particles (helium nucleus) fall into the category of high LET which means they do not travel far before

interacting, and in the case of alpha-particles their energy is deposited very near the place in which they are generated. Neutrons, which are essential for maintaining a fission chain reaction, have a neutral charge which allows them to easily penetrate the electron clouds surrounding other nuclei and cause other fission events. On the other hand, beta (b)-particles (electrons of nuclear origin) and gamma-rays fall into the category of low LET radiation since they are not direct forms of ionizing radiation, and gamma-rays in particular travel the farthest through materials before depositing their energy. Gamma-rays are a form of high energy electromagnetic radiation that originates in the nucleus and is released in the form of photons (discrete bundles of energy). They damage systems by ionizing atoms, yet they must first interacting with an atom which occurs less frequently due to the fact that they carry no charge. Charged particles leave a trail of excitation and ionization through the medium they transverse, which is great for generating heat. In a fission reaction the fission products generated can be unstable. Decay heat can be significant problem in fission reactors after the reaction is stopped since these unstable nuclides will decay at a delayed rate maintaining the presence of nuclear reactions with the core and perpetuating high core temperatures for long periods of time after shutdown (36:414). Once the photon-particle chain reaction is halted in a triggered isomer design, the heat production will stop shortly thereafter simplifying this problem (37) since the formation of charged particles will drop off rapidly with the cessation of gamma production.

Table 4 displays the quality factor (Q), and LET value for the various forms of radiation. These values are means by which radiation doses can be compared. For instance, a dosage of gamma-radiation must be 10 times the dosage of alpha-radiation

received to have a similar biological effect. As these values grow, the level of biological damage grows too showing that x-rays and gamma-rays are the least damaging form of radiation. They will also travel the farthest from the source, which is not advantageous for this application.

Table 4. Quality Factors for Various Types of Radiation (36:473)

Type of Radiation	***Q***	**LET, keV/micron**
x-rays and gamma-rays	1	3.5 or less
β -rays, E_{max} < 0.03-MeV	1.7	~7
Naturally occurring α -particles	10	53
Neutrons:		
Thermal to 1-keV	2	7
1-MeV	11	~53
7-MeV	7	~23

Radiation dose is measured in units of rads, which corresponds to the absorption of 100 erg/g of a substance for any form of radiation, and when multiplied by Q, the equivalent-dose, measured in units of rem, can be obtained (same is true of dose rate and equivalent-dose rate). While doses on electronic hardware should be kept as low as possible, it is proposed that dose values in the range of 0.01 to 2 rad/s (38) should be allowable.

Table 5. Typical Exposure Numbers (3:493)

Exposure	**Dose-Equivalent or Dose-Equivalent Rate**
Natural radioactive material in bones	0.034 rem/yr
Flight in Aircraft	0.001 rem/hr (9 km altitude)
Chest x-ray (lung dose)	0.01 rem
90-day space station mission	16 rem (NASA estimate)
Properly shielding nuclear space engine	10 rem/yr (3.17×10^{-7} rad/s for gamma-exposure)

Table 6. Acute Radiation Effects from Whole-Body Exposure to Gamma-Radiation (3:494)

Acute Irradiation Level (rem)	**Acute Somatic Effect**
15-25	Subtle reduction in white-blood-cell counts; not generally apparent from exposure for one person unless a blood sample was taken before the exposure
50	Reduction in white-blood-cell count after exposure; the count returns to normal in a few weeks
75	10% chance of nausea
100	10% chance of temporary hair loss
200	90% chance of radiation sickness; moderate depression of white-blood-cell fractions
400-500	50% chance of death within 30 days without extensive medical treatment
>600	Lethal to most people in 3 to 30 days; even with extensive medical treatment, death is likely within a few months from infection and hemorrhage
>10,000	Lethal within 24 hours from damage to central nervous system

2.2.2. Attenuation, Absorption, and Emission. The attenuation of x-rays and gamma-rays in various materials is very important to this study for a number of reasons. In Fig. 2, the fundamental differences between all the known forms of electromagnetic radiation

are shown. A shorter wavelength corresponds to higher frequency and higher energy photon according to

$$E_{photon} = hn_{photon} \quad [2]$$

$$n_{photon} = \frac{c}{l} \quad [3]$$

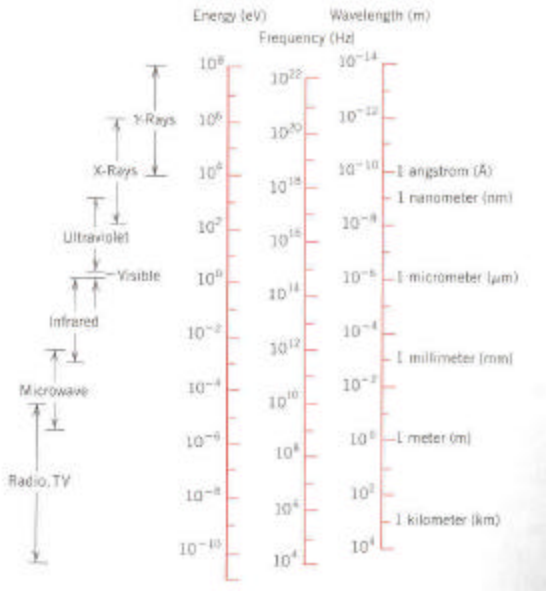

Figure 2. Electromagnetic Spectrum (39)

For a chain reaction to be maintained within the core, trigger photons, in a sufficient quantity, will need to be produced from interactions between the released gamma-radiation and core materials. In the interest of shielding, which will be covered in Sec. 2.2.3, it is important to understand the photon-particle interactions taking place in order to have safe, effective operation. Of prime importance, is the energy deposited by this electromagnetic radiation within the core. This is the means of heat production that

will drive propellant temperatures up and lead to high levels of performance. For a fission reactor approximately 82% of energy released will contribute to local increase in temperature (3:469) due to Coulombic interactions that take place between fission products and other charged nuclei. Gamma-rays are not charged particles and as a result they do not experience these Coulombic forces (36:90-101; 40:170-198). Once a gamma-ray interacts and generates a charged particle then its energy is deposited local to the area of this interaction.

There are three manners in which gamma-rays interact with materials that must be examined in nuclear core design problems. They are the photoelectric-effect, Compton scattering, and pair production. Pair production requires higher photon energies than generated in this case, so the focus becomes the other two forms of interaction. At gamma energies between 0.3 and 10 MeV, Compton scattering is the dominant mode of electromagnetic interaction. Below 0.3 MeV the photoelectric-effect dominates (3:472). In Compton scattering the incident photon is deflected from its path by an orbital electron, conserving both energy and momentum. The photon continues on with less energy in some new direction free to interact again, and the impacted electron recoils acquiring some kinetic energy from the photon. During this process the only energy deposited by the gamma-ray is the kinetic energy imparted to the electron. In the case of the photoelectric-effect, for which the probability of occurrence will increase as photon energies decrease, the photon will be absorbed and an orbital electron will be ejected from the atom. Thus a charged particle is now released, with energy equal to that shown in Eq. [4].

$$E_{particle} = E_{photon} - E_{ionization} \qquad [4]$$

All three processes by which gamma-radiation interacts with materials transfer energy to charged particles. Due to the Coulombic interactions discussed earlier, these particles moves only a short distance before their energy converts to heat (36:472). In order to capture the energy of released gamma-rays, the material and configuration surrounding the isomer must be capable of causing enough photon-particle interactions that energy is deposited locally. High efficiencies of energy deposition will no doubt lead to lesser requirements for power production by the fuel materials. The requirement then becomes effectively removing this deposited energy with propellants to maintain steady core operating temperatures. In addition, there is a need to maintain a chain reaction within the core which means trigger photons will need to be generated during this process to avoid including a source for this type of radiation in the rocket design.

The vacancy left by the departing electron from the photoelectric-effect can result in the emission of radiation in the form of characteristic x-rays or the ejection of Auger electrons. The energy of these released x-rays is determined by the difference in binding energy of the ejected electron and the electron that takes its place by transitioning down from a higher shell (40:43). This process is known as x-ray fluorescence. In addition to finding materials that fluoresce at the desired photon energy (9 to 13, ~40, ~60 keV), the number of x-ray photons generated is extremely important to maintaining a chain reaction if the probability of triggering decay is only 0.2% (10), as stated by Collins. In addition, this process competes with the ejection of Auger electrons, which is more common in elements with low atomic numbers (40:45). Auger electrons are emitted instead of a photon, and in some materials Auger cascades can occur releasing several electrons as transitions continuously occur. Should an element with low atomic number be necessary

for supplying the required x-ray fluorescence controlling this process will require more attention.

Important to all of this are the mass attenuation (m/r), mass energy-absorption (m_A/r), and mass energy-transfer (m_{tr}/r) coefficients of materials when exposed to electromagnetic radiation of various energies. Tables 19 and 20 in Appendix B contain some of these values for the materials of interest in this study. These values simply need to be multiplied by the material density to yield the linear coefficients (m and m_A). The linear mass attenuation coefficient is a measure of the photons statistical interaction probability per distance traveled, where $1/m$ represents the average distance traveled by a photon before interacting (40). The linear mass energy-absorption coefficient is a measure of the photons statistically probability of depositing its energy per distance traveled. The linear mass energy-transfer coefficient does not include the energy emitted in the form of bremsstrahlung radiation, and the relation between it and μ_a is found in the following equation.

$$m_a = m_{tr}(1-g) \qquad [5]$$

In Turner (40:193), g is defined as "the average fraction of initial kinetic energy transferred to electrons that is subsequently emitted as bremsstrahlung."

2.2.3. Shielding & Reflecting. An important point is that short wavelength electromagnetic wave emission does not result in the release atomic particles or residual unstable radioactive states. The advantages of this will likely be evident when determining the amounts of shielding needed for safe operation. It is likely that all of the

released photons will not be absorbed within the core, and some may make their way beyond the core containment vessel. Therefore, a means of shielding will be needed to protect surrounding equipment from the adverse effects of interaction with the decay products. As discussed previously, x-rays and gamma-rays easily penetrate most materials which will no doubt be one of the major challenges in the overall design of a Triggered Isomer Core (TIC). The mean free path for interaction of a 600 keV gamma photon in lead is approximately 0.7 cm, while the mean free path for absorption extends over 1 cm. X-rays penetrate significantly less, as an approximate mean free path for the absorption of a 10 keV photon in lead is about 705 μm. Mean free path calculations for various materials and various photon energies are tabulated in Table 21 in Appendix B.

In a conventional fission reactor the reaction is maintained at a critical state through moderators, control rods and reflectors that maintain the necessary neutron population and energies within the reactor. Preliminary experiments (9; 10; 28; 29) indicate that low-energy x-rays are the key to unlocking the energy stored in the $^{178}Hf^{m2}$ isomer so it is likely that their population within the reactor will become essential to establishing and maintaining a chain reaction. While x-rays can be reflected to some degree if their incident angle is very small (mirrors are positioned nearly parallel to the source), gamma-rays are absorbed in all materials and no means of reflecting them seems to exist at present (41). Gamma-ray telescopes must rely on techniques to simply count the gamma-rays incident from a source in outer space. The inability to reflect gamma-rays becomes important when the realization is made that any photons not initially absorbed within the core will need to be attenuated in the shielding material. In addition

there will be an energy loss associated with this that will be an important consideration in reactor design.

2.2.4. Environmental Laws and Regulations. In designing a system that results in the release of radioactive products, engineers will be faced with a long, detailed, and drawn out process for the approval to design, test, and operate such a system. The benefits of such an engine must outweigh the potential risks. The risks of flying such a rocket within the atmosphere, whether it is operating or simply being transported to power later stages must be assessed with an emphasis on environmental impact should an accident occur. If the leap is made to manned systems; the crew must be adequately protected during operation and in the event of a malfunction. The hazards associated with construction, storage, and launch pad operation must be assessed and a number of people present during safety reviews and approval processes must be convinced that the design can be operated safely. An example of the Nuclear Safety Review and Launch Approval Process is shown in Fig. 3, and until this process is complete normal launch operation cannot proceed.

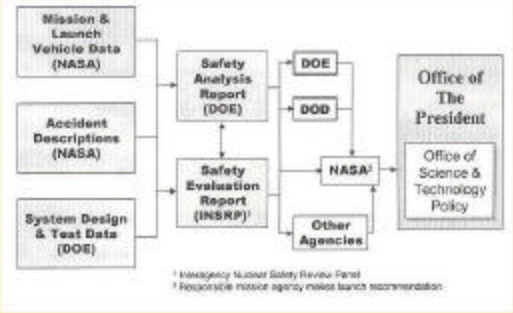

Figure 3: Nuclear Safety Review and Launch Approval Process (42)

The largest area of contention is likely to be the classification of this technology. While a nuclear reaction is not taking place, radiation is being emitted, meaning that a similar process if not the same will be probable for this technology. Gamma-radiation also travels farther than any of the other types of radiation created during the fission reaction. Addressed in this work will be the shielding necessary for utilizing such a design and the likely exposure received by the rocket's surroundings.

2.3. Nuclear Rocket Development

With the advent of the first controllable fission chain reactor in 1942, the far-fetched idea of utilizing atomic energy as a means of power in space became more than just a dream. Throughout history many programs in the U.S., Russia, and European nations have made greats strides in making this dream a reality. While much research has been accomplished to date, nuclear thermal power has still not made a successful transition to spaceflight. It has had to battle strict environmental laws, lack of funding, the end of the space race, and support that disappeared just as systems reached a level of maturity (1; 43). Some of the most recognizable gas-cooled nuclear space reactor programs deemed probable for adaptation to usage of triggered isomer energy were researched and are described in the next section.

2.3.1. Types of Space Nuclear Reactors. There are many differences between the terrestrial reactors used to provide electricity here on earth, the reactors used to power some naval vessels, and those reactors that will be most applicable to space operations. The operating environment and requirements placed on reactors launched into space will

dictate that they be compact, capable of safe modes during launch, capable of starting in space, be extremely reliable, and make use of gases or liquid metals for coolants. With the choice of constructing a solid, liquid, or gaseous-core reactor, the solid-core is the simplest and most well understood reactor making it the first choice for a space nuclear power system. It has the disadvantage of lower propellant temperature when compared to the other two designs but, nonetheless, was chosen on the basis of documented engineering experience (3:452-459; 4:12-19; 5; 6; 18; 19; 20; 21). With the type of reactor chosen the means for harnessing its power becomes the central area of focus. The two most popular means by which this is done are known as nuclear thermal and nuclear electric propulsion. Nuclear thermal propulsion involves heating a propellant directly and accelerating the flow through a nozzle to produce thrust. Nuclear electric produces heat energy as well, but uses power conversion systems to create electricity which can power both onboard systems and propulsion devices such as ion thrusters. Much greater levels of specific impulse are available with nuclear electric propulsion over nuclear thermal, which makes it an attractive choice for long duration space mission. Nuclear thermal propulsion, though, has the benefit of high thrust levels and the ability to affect the vehicles velocity on short time-scales, which make it a more attractive choice for operating in the presence of large gravitational forces and on quick turn-around missions. In Sec. 2.3 the history of space nuclear fission reactors is covered from which designs for a new system utilizing isomer decay as the heat source can no doubt benefit.

2.3.2. Nuclear Engine for Rocket Vehicle Application (NERVA). The ROVER/NERVA program is likely the United States' most highly publicized nuclear rocket program. The ROVER research portion of the effort began in 1955 as a program aimed at powering Intercontinental Ballistic Missiles (ISBMs) with the goal of developing a flight-rated thermodynamic nuclear rocket engine with 75,000 pounds of thrust (44). The program produced several reactors that made it all the way through the testing stages of development. The reactors used uranium-235 with graphite moderators, beryllium reflectors, and hydrogen as the propellant (3:452; 5; 6; 18; 44; 45). The fuel elements were hexagonally shaped with the uranium fuel dispersed in a variety of manners within a graphite matrix. Coolant channels flowed through these elements and utilized a protective coating to prevent erosion of the fuel elements in order to maintain a fixed configuration throughout the reactors operation. Rotary drums containing neutron absorbing material were used to control the fission rate while a surrounding reflector and pressure vessel maintained the presence of the fission products and necessary reactor pressure. Of these the KIWI series of reactors successfully demonstrated the basics of building a nuclear rocket. The program was able to overcome the initial difficulties of graphite erosion through the use of niobium carbide coatings, make a successful transition in fuel material from uranium oxide (UO_2) to uranium carbide (UC_2), and eliminate the internal vibrations causing the fuel elements to fracture. Much larger reactors were developed in the Phoebus series with the final test operating at over 4,000 MWt (5). The coating protecting the graphite from H_2 corrosion was further improved in this test series to a niobium carbide-molybdenum mixture. With the Pewee series of reactors aimed and building a more compact reactor power densities were increased and

the coating was improved to a zirconium carbide material. NASA took over the program in 1958 and by 1960, in coordination with the Atomic Energy Commission (AEC); the NERVA portion was commissioned along with the Space Nuclear Propulsion Office to manage it (44). This program went beyond the current efforts of researching reactor design and was aimed at producing an actual space nuclear reactor that could be deployed on missions. The Nuclear Reactor Experiment (NRX) began testing in 1964 and sought to demonstrate that a reactor could be built that was capable of withstanding vibration and shock loadings consistent with launch vehicle operations. The program culminated with the testing of the XE-Prime reactor which was the first to be fired like an actual rocket with its exhaust end facing downward. Reliability, restart capability, predictability, controllability and structural integrity were all of interest in this testing and the final reactor design made significant progress towards all of these goals (5). The XE-Prime testing achieved power levels as high as 1,100 MWt, but once again was faced with the problems of cracking fuel bundles and eroding graphite despite the evolution of coating materials (5). The program ended in 1972 but not before a number of different reactor designs were tested at AEC's Nuclear Rocket Development Station in Jackass Flats, Nevada. The ROVER & NERVA program generated a proven reactor design that was actually slated for a mission to Mars after the U.S. successfully landed on the moon. The end of this program came about not because of engineering failures or insurmountable scientific hurdles, but because of changes in government spending and a shift in space priorities. With a renewed interest in NTR technology, improvements to the old NERVA designs have been realized with advances in cooling, material, and manufacturing technologies (18).

2.3.3. Particle Bed Reactor (PBR). In the early 1980s the idea of using a PBR to increase the surface area available for heating a propellant began to grow in popularity (21). A PBR consists of a bed of spherical fuel particles protected from the propellant flow by layers of graphite and zirconium carbide. The particles are housed between two concentric porous cylinders called frits. The propellant flows radially in through the outer (cold) frit, is heated by the fuel particles in the packed bed, flows out radially through the inner (hot) frit, then flows axially out of the fuel element, and is then expanded through the nozzle to produce thrust. A variable number of fuel elements can be included in a hexagonal arrangement, surrounded by a moderating material to control the reaction. A reflector and pressure vessel surround this arrangement of fuel elements. In 1987 the Strategic Defense Initiative Office initiated the Space Nuclear Thermal Propulsion (SNTP) program which assumed control of the development of this technology (21). This program was transitioned to the Air Force in 1991 and only lasted until 1993. No full-scale engine tests were conducted as with the ROVER/NERVA tests series, but the concept was proven through a series of smaller tests. Fuel tests with hydrogen reached temperatures as high as 3,000 K, where the highest temperature reached in the ROVER/NERVA experiments was 2,650 K (3:453). Other achievements of this program were tests of single fuel elements, criticality experiments for a prototype 1,000 MW core, tests with power densities as high as 40 MW/liter, various mission designs, and verified computer codes (3:454).

2.3.4. CERMET. Fast fission nuclear reactors have also been given some attention for possible space nuclear reactor designs. These types of reactors do not utilize a moderator

to control the fission rate because they operate on a fast fissioning spectrum at energy levels above 1 MeV (3:455) and rely on higher uranium enrichment within the fuel elements to allow self-sustained fission. The CERMET reactors, as they are known, contain uranium dioxide fuel particles embedded in a metal matrix of molybdenum and uranium or tungsten, rhenium, and uranium. The term cermet is simply used to classify such a metal matrix. Both tungsten and rhenium have high melting points and high atomic numbers meaning that they are good materials for withstanding core temperatures and for absorbing the radiation given off by the fuel source. Molybdenum has a relatively high melting temperature and can be used in the cooler regions of the reactor to decrease the reactor mass. From 1961 to 1967 Argonne National Laboratory conducted a program to develop just such a reactor (5). Unlike the ROVER/NERVA series no engines were built or tested in this program but a longer operating life, restart ability, low sensitivity to temperature cycling, and better compatibility between hot hydrogen and the fuel were all realized as potential benefits of the development of this technology. Fast reactors are also generally smaller and lighter than thermal reactors, but this can vary based on the composition of the cermet matrix.

2.3.5. Isotope Thermal Thrusters. As a result of the work being done under the ROVER program, a series of miniature direct cycle nuclear systems were spawned (46:103). A very simple form of heating a propellant was realized by utilizing natural alpha, beta, or gamma-radioactive decay. In general these systems consist of a radioisotope capsule with some type of decay particle absorbing structure which is heated by the radioactive decay and able to transfer its heat to the propellant passing over it

before the propellant is expanded out a nozzle. The Marquardt Corporation worked on a gamma-heated system under USAF sponsorship which utilized thick tungsten heating elements on the outside of the capsule to capture the radiated energy (46:101). The POODLE thruster which had a and b sources also had both active and passive thermal control systems. The active control system which was able to expose the heat source to space when propellant flow was cut off had calculated thermal efficiencies near 90% (46:102). Though these were very low thrust systems due to their dependence on a natural rate of radioactive decay, they reinforce the idea that gamma-radiation can be captured within a core and used to heat a propellant.

3. Methods and Theory

The basic goals when designing a heat source for space propulsion, whether it powers a launch vehicle or a deep space probe, can be very similar. Regardless of the application, engineers strive to design a system that can effectively and efficiently transfer heat to a propellant through radiation and convection. Effective shielding is incorporated to allow for a safe operating environment. The mass of this heat producing core and its required shielding are minimized to preserve payload capabilities. In the case of a nuclear or triggered isomer core, the design configuration must be worked out with great care so that a chain reaction can be maintained and controlled in such a fashion that the melting temperatures of the core materials are not exceeded. Also a means for starting and, in some instances, stopping the chain reaction on demand could be very beneficial.

3.1. Assumptions.

3.1.1. Isomer Decay Process. Due to the infancy of controlling isomer decay and the lack of existence of similar systems, two general assumptions needed to be made in this study to limit the research in some manner.

1. A chain reaction and the heat generation rate within the core can be controlled and steady-state operation is achievable. This includes a means for generating and maintaining the necessary trigger photon population.

2. Production of the isomer $^{178}Hf^{m2}$ can be escalated to at least the 100 g/yr goal (25).

3.1.2. Rocket Configuration. There are a multitude of systems on a rocket that could be affected by a change to the propulsion system, and the goal of this study was not to design an entirely new rocket configuration. Instead, the current system was assumed to remain, for the most part, unchanged. Both stages of the Delta IV-H are cryogenically fueled and small modification to the storage and handling system, such as eliminating the liquid-O_2 segment and expanding the liquid-H_2 storage area, were imagined. In both the gas-generator (stage 1) and split-expander (stage 2) propellant feed systems used in the current system, regenerative cooling of the thrust chamber structure pre-heats the propellant (3:201). For the purposes of this study all the propellant was assumed to be in gaseous state by the time it reaches the turbine. This may lead to lower chamber pressure, (3:200) below what is desired in the actual design, but optimization of this value will not be addressed in this study. The nozzle segments, designed specifically for the vehicles flight profile, were not altered and the expansion ratio used on the current vehicle was carried over to this study.

3.2. Nuclear Fission Reactor Performance.

Like a fission reactor, the Triggered Isomer Core (TIC) will benefit from the ability to use a single propellant for the dual purpose of cooling the reacting materials and providing the thrust necessary to propel the vehicle through space. The first step in this process was to use the information gathered on the NERVA, CERMET, and PBR designs

(Table 1) to baseline the potential for improvements in performance by instituting fission reactors as the propulsion sources in space launch and orbit maneuvering vehicles. The performance of a TIC measured against these fission reactors was then addressed. Each reactor was examined, through use of the process outlined in Sec. 3.3, to verify that it could satisfy the requirements of the missions (Table 2) and to determine what level of improvements are possible over the current systems. The data on the reactor designs does not necessarily represent the best that can be achieved with these designs, but it was used to show that significant improvements will still result, lending weight to the argument for not relying solely on chemical propulsion for high thrust missions.

3.3. Rocket Fundamentals.

3.3.1. Nozzle Analysis. An excellent preliminary design process is presented in the text by Humble, Henry, and Larson (3). The process outlined there was used in this research (Sections 3.3.1-3.3.4) to perform an analysis of a rockets performance and power requirements knowing the conditions listed below.

a. Propellant
b. Thrust (F)
c. Nozzle expansion ratio (e)
d. Initial vehicle mass (m_i)
e. Payload mass (m_l)
f. Velocity change requirement (Δv)
g. Gas temperature at core inlet & outlet (T_1 and T_2)
h. Core chamber pressure (P_c or P_2)
i. Estimated pressure drop through reactor (P_{drop})
j. Mach number at core outlet (M_2)

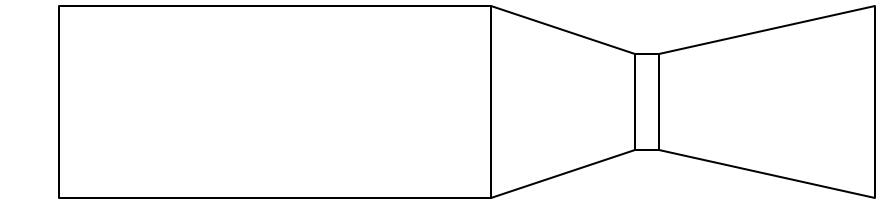

Figure 4. Position within Engine as denoted by Subscripts

The following analysis is essentially just an examination of rocket nozzle performance with the following assumptions.

1. Isentropic flow (reversible & adiabatic) through the nozzle.
2. Negligible friction, fluid viscosity, and heat transfer to nozzle walls.
3. One dimensional, steady, frozen flow.
4. Propellants are treated as perfect gases

Propellant specific heats (c_p) were calculated from equations obtained from Humble, Henry, and Larson (3:460) and a Chemkin data file (47). Knowing the specific heat value, the following expression can be used to obtain the ratio of specific heats (g).

$$g = \frac{c_p}{c_p - Ru} \qquad [6]$$

As stated earlier, the core inlet temperature in every case was assumed to be 300 K and under this assumption the propellants used in this study are all gases at that temperature. Knowing the temperature and pressure conditions, and the flow Mach number at the core outlet, the stagnation properties can be obtained using the following

isentropic relations. The importance of Mach number is discussed in Sec. 3.3.2 of this work.

$$T_o = T\left(1 + \frac{g-1}{2} M_2^{\,2}\right) \qquad [7]$$

$$P_o = P(1 + \frac{g-1}{2} M_2^{\,2})^{\frac{g}{g-1}} \qquad [8]$$

Acoustic (a_o) and characteristic (c^*) velocities are now needed and can be determined via the following equations.

$$a_o = \sqrt{g(\frac{Ru}{MM})T_o} \qquad [9]$$

$$c^* = \frac{a_o}{g(\frac{2}{g+1})^{\frac{g+1}{2g-2}}} \qquad [10]$$

The Mach number at the nozzle exit must be iteratively calculated using the following equation.

$$0 = M_3 e - [(\frac{2}{g+1})(1 + \frac{g-1}{2M_3^{\,2}})]^{\frac{g+1}{2g-2}} \qquad [11]$$

Now the ratio of exit pressure (P_e) to chamber pressure (P_c) can be found, and knowing either the chamber or exit pressure will determine the value for the other.

$$\frac{P_e}{P_c} = \left[1 + \frac{(g-1)}{2} M_3^{\,2}\right]^{\frac{g}{1-g}} \qquad [12]$$

The nozzle exit temperature (T_e) is available through another isentropic relationship once the exit pressure is determined.

$$T_e = T\left(\frac{P_e}{P}\right)^{\frac{g-1}{g}} \qquad [13]$$

And now the important performance characteristics such as specific impulse (I_{sp}), mass flow rate ($\dot{m}$), and nozzle exhaust velocity (v_e) can be calculated.

$$I_{sp} = \frac{c^* g}{g_o}\left[(\frac{2}{g-1})(\frac{2}{g+1})^{\frac{g+1}{g-1}}\{1-(\frac{P_e}{P_o})^{\frac{g-1}{g}}\}\right]^{0.5} \qquad [14]$$

$$\dot{m} = \frac{F}{I_{sp} g_o} \qquad [15]$$

$$v_e = I_{sp} g_o \qquad [16]$$

Pressure thrust has been neglected in this analysis since that level of exactness was not needed for the comparisons made here.

3.3.2. Conservation of Mass. Flow through a core, as long as the flow channels can be modeled as straight circular ducts and the flow is steady, can be analyzed using the conservation of mass law. The importance of this stems from the desire to have a low flow velocity throughout the core (definitely subsonic) and in the region of mach number 0.2 to promote heat transfer and avoid the loss effects of flow induced vibration (3:463). Thus in this study the Mach number of the propellant exiting the core was set at 0.2 to satisfy this requirement leading to flow at the inlet in the range of 0.05 to 0.16 for the various reactor designs. At the core outlet the velocity of the flow (v_2) is needed first.

$$v_2 = M_2 a_2 \qquad [17]$$

For a constant area duct we then have a conserved quantity (G) based on the mass flow in equaling the mass flow out.

$$G = \rho_2 v_2 \qquad [18]$$

The equation above does not apply to the PBR design since the flow area changes along the length of the flow passage, but with the documented value of the pressure drop, no major issues are raised in the analysis. It is just not possible to calculate v_1 and M_1 for the PBR design without more information on the flow geometry. The reactors are assumed to have a 10% (Enhanced NERVA), or 53.7% (CERMET) pressure drop (P_{drop}) due to flow losses (3:463). In this analysis this pressure drop is given as a percentage of the achieved chamber pressure at the core outlet (P_2). Knowing the pressure at the core outlet (P_2) allows us to work backwards and to calculate the required pressure at the core inlet (P_1).

$$P_1 = P_2 + P_{drop} P_2 \qquad [19]$$

The same process shown in Sec. 3.3.1 was then used to find γ_1, a_1, ρ_1 (at the core inlet), and the flow velocity and Mach number at the heater inlet can be determined in the same manner as shown in Eqs. [17] and [18]. The same isentropic relations used in Sec. 3.3.1 are also used to calculate the stagnation properties of the propellants at the reactor inlet.

3.3.3. Power Calculations. Boundaries have been set on the propellant temperature at the core inlet and outlet. The temperature of the propellant entering the core is 300 K and at the reactor outlet it is going to vary based on the properties of the propellant and the core's ability to transfer heat by convection to the propellant. Solid cores are typically

limited to the melting temperatures of the materials from which they are constructed. For the ceramics used in the reactors considered here that is somewhere in the range of 3,100 to 4,200 K (Table 18 in Appendix A). A derivation of the energy equation leads to the following expression for determining the power necessary to heat a particular mass flow rate of propellant to the desired temperature. This is the power (P_{core}) that must be produced and transferred to the propellant within the core for this technology to be successful.

$$P_{core} = \frac{\dot{m}}{MM}(h_n + \int_{T_1}^{T_2} c_p \, dT) \qquad [20]$$

The above expression will yield P_{core} in kW and must be multiplied by 1,000 to express the value in watts.

3.3.4. System Sizing. The level of thrust required is determined by the mission, which will directly drive the mass flow rate required through the core (Eq. [15]). To increase a rocket's thrust, one must increase the mass flow rate of propellant through the reactor. A new relation can now be used to show the link between the chamber pressure (P_c) and the nozzle throat area dimension (A_t), which will directly affect the engine size and weight.

$$A_t = \frac{c^* \dot{m}}{P_c (10)^6} \qquad [21]$$

The characteristic velocity (c^*) is a function of the propellant and its heated temperature, and the use of this equation requires the assumption of isentropic, 1-D, steady flow of a perfect gas. For a given expansion ratio, a larger throat area will dictate a larger nozzle

exit area and overall increase in the size of the rocket nozzle. As the rocket nozzle grows in size it grows in weight, so maintaining large values of P_c can lead to smaller rocket nozzles. On the other hand, larger values of P_c also lead to increases in the mass of the pressure vessel surrounding the core so there is a trade off. This vessel's purpose is to maintain high pressure throughout the core and its mass (m_{pv}) can be estimated with the following relation (3:272).

$$m_{pv} = \frac{2P_c(10)^6 V_{pv}}{9.81 f_{pv}} \qquad [22]$$

This relation is derived in Humble, Henry, & Larson (3) for estimating the storage tank mass since the shape of a reactor pressure vessel is similar to a propellant tank. For nuclear fission reactors a typical value for P_c is between 3 and 10 MPa (3:502). As shown later, flight within the atmosphere will not be covered in great detail, but it is important to note that chamber pressure has another important effect on vehicles flown in regions of high atmospheric pressure. Flow separation within the nozzle is typically controlled by adjusting the chamber pressure and nozzle expansion ratio to achieve values an exit pressure between 15 and 45 kPa (3:205). In that case more emphasis should be placed on this value.

3.3.5. Mission Feasibility. The goal here is to determine if the rocket design is feasible for the intended segment of the mission. Each segment has its own velocity change (Δv) requirement, and each rocket segment will have restrictions on propellant mass (m_p) and

gross mass at liftoff (m_i). The amount of propellant (m_p) needed to achieve a required Δv with a certain system is obtainable through the following two relationships.

$$m_f = m_i(e^{\frac{-\Delta v}{v_e}}) \quad [23]$$

$$m_p = m_i - m_f \quad [24]$$

The first relationship shown above is a variation of the ideal rocket equation and it is used with the effects of the pressure thrust being neglected. The variable m_f is the final mass of the system upon achieving the desired change in velocity (Δv). Specifically for this study the propellant mass savings (m_{extra}) achieved by using a propulsion source capable of higher I_{sp} values must not be offset by the mass of that source plus the shielding requirements based on its radiation output. The symbol m_{prop} designates the mass of propellant carried by the current system and (m_{extra}) is simply obtained by the following relationship.

$$m_{extra} = m_{prop} - m_p \quad [25]$$

The quantity must be positive in order to continue else the replacement of a chemical system doesn't make sense; better performance is desired. The inert mass fraction (f_{inert}) can be obtained in the following fashion by first determining the structural mass of the rocket (m_s).

$$m_s = m_f - m_l \quad [26]$$

$$f_{inert} = \frac{m_s}{m_p + m_s} \quad [27]$$

Another process generates an equation for propellant mass using a combination of mass equations and the ideal rocket equation. The result is an equation with the following term as the denominator.

$$1 - f_{inert} e^{\frac{\Delta v}{I_{sp} g_o}} > 0 \qquad [28]$$

A propellant mass that is infinite or less than zero is physically impossible, so the equation above serves as a check for feasibility.

Thrust-to-weight (*F/W*) ratio is also an important rocket parameter, especially for launch systems. A launch vehicle's initial thrust-to-weight ratio must be greater than one for the vehicle to leave the ground. Typical values for this are in the range of 1.2 to 1.5 for launch vehicles, and usually greater than 0.2 for upper stages (3:17-18). If rocket payloads can withstand the g-forces of high thrust, then a spacecraft will experience a lesser values of Δv loss due to gravitational forces. For the purposes of this study a high *F/W* ratio will be considered a positive characteristic.

3.3.6. Rayleigh Line Analysis. An investigation of the probability for thermal choking was also conducted. The equation used in this analysis (48:246) requires the assumption of a perfect gas and constant specific heats, so an average value of the specific heat throughout the reactor was used. First the stagnation temperature at Mach 1 must be calculated.

$$T_o^* = \frac{T_{o2}}{\left(\frac{T_{o2}}{T_o^*}\right)} \qquad [29]$$

The quantity T_{o2}/T_o^* has tabulated values for given Mach number (48:669). Equation [30] solves for the maximum amount of energy (q_{max}) that can be added to a fluid before thermal choking occurs. That is the condition that describes the propellant being accelerated to Mach 1 by the heating process alone, and this will have serious repercussions on the flow through the nozzle. Supersonic flow entering the nozzle's diffuser section will decelerate resulting in large drop in propellant exhaust velocity. As the exhaust velocity decreases so does the specific impulse.

$$q_{\max} = T_{o1} c_{p_{avg}} \left(\frac{T_o^*}{T_{o1}} - 1\right) \qquad [30]$$

To get the maximum power (P_{max}) multiply q_{max} by the mass flow rate.

$$P_{\max} = q_{\max} \dot{m} \qquad [31]$$

3.4. Hafnium Requirement.

The determination of the minimum amount of hafnium isomer that must decay to supply the power required is calculated with the following series of equations. This amount of isomer may not be sufficient to sustain a chain reaction, but nevertheless provides a starting point for estimating fuel requirements. The burn rate (cr) is first determined knowing both the power requirements of the core (P_{core}) and the energy stored by the hafnium isomer (1.3 GJ/g).

$$cr = \frac{P_{req}}{1.3 \frac{GJ}{g} * 1000} \qquad [32]$$

Burn time (t_b) is calculated knowing the propellant used and its mass flow rate.

$$t_b = \frac{m_p}{\dot{m}} \quad [33]$$

From these two quantities the mass (m_{Hf}) and volume (V_{Hf}) of hafnium required can be obtained through use of the following two equations.

$$m_{Hf} = t_b * cr \quad [34]$$

$$V_{Hf} = \frac{m_{Hf}}{r_{Hf}} \quad [35]$$

3.5. Energy Deposition and Fluorescence.

Due to the current state of triggered isomer research, it is not likely that models exist for simulating a chain reaction within such a material, and no models were discovered in this study. Instead the approach taken in this study was to examine various materials (those used in the fission designs and other likely candidates), and assess their abilities to, not only, absorb photon energy, but also to fluoresce at the desired photon energies. Fluorescence is a process by which an atom absorbs a photon and re-emits a photon of different wavelength.

For each of the nuclear core designs the power required by the core (P_{req}) was assumed to be the power required to heat a particular mass flow rate of propellant to a desired temperature based plus power escaping due to radiation from the core. P_{req} is actually greater than what is needed to heat the propellant to the desired temperature and the efficiencies for this process of these nuclear cores was estimated from the data available (Table 1) by comparing their power values against the power needed to heat H_2

to the listed temperature achieving the listed thrust value. The actual calculation of these efficiencies is displayed in Appendix H (H.1).

Achieving these levels of efficiency with a TIC, however, will require additional material within the core due to the mean free paths in materials for gamma-ray photons (Table 21 in Appendix B). The *Nuclear Engineering Handbook,* by Etherington, (11:7-66) provides a process by which this efficiency can be roughly estimated. To carry this out, the core was envisioned to be a point source gamma emitter producing photons of only 500 keV (E_o). A spherical layer of material is placed around this source at a distance R, with a thickness x as shown in Fig. 5.

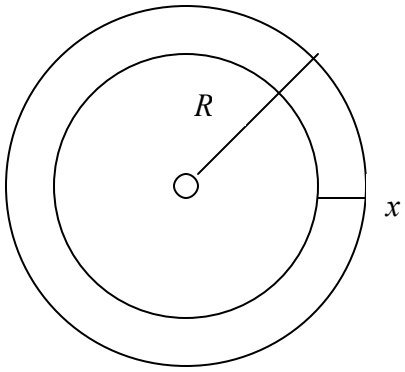

Figure 5. Core Simplification to a Spherical Body

In order to calculate the energy at a being deposited at a distance R from the source beyond a thickness x of material the following expression can be used.

$$H(R,x) = 1.062(10)^{-6} m_a E_o B_a(mx)\Gamma^o(R,x) \qquad [36]$$

The linear energy-absorption coefficient (m_A) takes into account the most probable forms of photon-particle interaction (photoelectric-effect, Compton scattering, and pair production), and as stated earlier, will vary with the energy of the photon and type of

material being considered. Table 20 in Appendix B lists the mass energy-absorption coefficients for a variety of materials subject to various incident photon energies. The mass energy-absorption coefficient is simply multiplied by the material density (r) to obtain the linear energy-absorption coefficient. In order to generate values for H (the power of the gamma radiation at the outer surface of the enclosing layer of material) the current density of uncollided photons (Γ^o) and the buildup factors for energy absorption (B_a) are required. The former can be determined in the following fashion.

$$\Gamma^o(R,x) = \frac{Se^{-mx}}{4pR^2} \qquad [37]$$

The source strength (S) was obtained by dividing an estimated core power by 500 keV per photon to obtain the number of photons being produced per seconds. This should allow for a worse case estimate since most of the photons produced during the decay of $^{178}Hf^{m2}$ have less energy than this. For the relaxation lengths (mx) listed in Etherington (11) and with knowledge of the linear attenuation factors for various materials (Table 18), layer thickness for the listed relaxation lengths can be found. Each thickness will have associated with it a buildup factor (B_a). This process is demonstrated in Appendix I for lead and tungsten. Since data on tungsten was not available in the tables it was obtained by iterating between two of the material listed in the table. The fact that buildup factors are linear functions of the atomic number allows for this. The volume of material absorbing the radiation was then used to provide the mass of material required and also determine the total power being radiated beyond the surrounding layer of material. For various amounts of material it is possible to determine a probable efficiency for this

energy release. Core masses will likely need to be increased, by at least these amounts calculated, if energy deposition within the core is to be achieved.

A materials ability to absorb incident gamma-radiation and subsequently emit x-ray photons of the energy needed to sustain a chain reaction within the TIC was examined using only the listings of x-ray transition energies for various materials (49). A material's x-ray photon emission energy (or transition energy) is determined by the difference between the ionization energy of ejected electron and that of the electron that transitions down from a higher orbit. The energies listed in the tables provided by the National Institute of Standards and Technology (NIST) are not necessarily representative of achievable photon energies as some may occur with very low probability. For this to work the probabilities for ionizing just the right orbital electron followed by the transition producing photons in the isomer's range of sensitivity to triggering will need to be very high since only a limited number of gamma-photons are emitted from $^{178}Hf^{m2}$ as it decays. Materials were chosen from these listings as potential sources of trigger photons in a TIC based on a combination of their potential for emitting photon within the desired range and their level of attenuation. It would be desirable to have the photons produced reach the isomeric material in the core before being absorbed near the point of their emission (34).

3.6. Radiation Shielding.

The shielding analysis carried out here focuses on shielding for biological and equipment protection purposes and not on heat shielding which is used to protect the pressure vessel surrounding the core from excessive heat (36:548). Radiation shielding

in general is dependent on many factors such as the power and type of radiation emitted, the distance between the radiation source and those components sensitive to radiation, and the level of sensitivity of those components (3:494). For the purposes here the mission is unmanned eliminating the need to protect humans, but in the case of the 1st stage vehicle shielding may be necessary to prevent a harmful release into the environment. The assumption of radiation hardened electronics and payload is made in this study, to a level able to withstand doses up to 0.01 rad/s (38). Safe doses for human are in the area of 1 μrad/s (2:66), and this level of radiation exposure will be examined to view how shield weights can vary with the level of radiation exposure tolerable.

3.6.1. Nuclear Fission Shielding. Shielding from the harmful effects of a nuclear fission reaction is somewhat different from shielding against a gamma release alone. Present in the fission reaction are fast moving neutrons and alpha particles which are high LET forms of radiation. These particles have high probabilities of interaction with other particles within the medium they are passing through. It is also not always desirable to absorb all of this radiation so a variety of materials can be used; one is beryllium to reflect neutrons and help maintain their population within the core, and another is lithium hydride used to slow down neutrons as well as take some part in their attenuation. A basic flat shield design, shown in Fig. 6, is capable of reducing the gamma ray flux by a factor of 0.00105 and the neutron flux by a factor of $4.0(10)^{-9}$ (3:495). The image shown is a cross-sectional view showing the thickness of the shields material layers of beryllium (Be), tungsten (W), and lithium hydride (LiH_2).

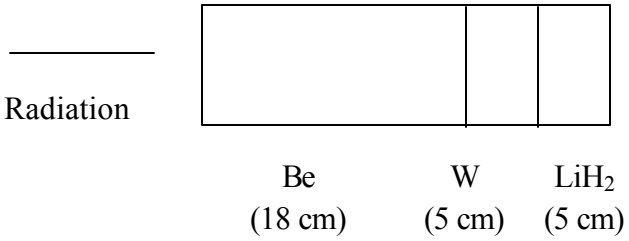

Figure 6. Typical Fission Reactor Shadow Shield (3:496)

The dimensions of this shield can be adjusted to achieve further levels of reduction, but as shown such a shield would have a shield loading factor of 3,500 kg/m^2, and calculation of the shield weight would simply require multiplying the shields surface area by this value. For case where a shadow shield is place on top of the reactor to shield the remainder of the spacecraft from escaping radiation, the radius of this shield can be approximated to have the same radius of the reactor it is shielding.

3.6.2. Gamma-Ray Shielding

The method used for calculating the radiation shielding necessary for protection from a gamma-ray release was taken from Turner (40:368) and Lamarsh (36:549). This method also treats the core as a point source emitter. The dose rate ($\dot{D}$) received at a distance r from the source can then be determined knowing the mass energy-absorption coefficient for air (m_A / r) and the rate of energy being released in the form of gamma-rays (CE).

$$\dot{D} = \frac{CE}{4pr^2}\frac{m_A}{r} \qquad [38]$$

The values for the mass energy-absorption coefficient vary based on photon energy, but for air the value is pretty consistent across the range of 100 to 600 keV photons. An important consideration in the actual design will be the medium separating the spacecraft from the energy source since this will affect the dose rate by altering (m_A / r). Once the dose at a distance without shielding is known the shield relaxation length (mx) can be determined with the following relation including a buildup factor (B) that takes into account the scattering of photons within the material.

$$mx = -\log\left(\frac{\dot{D}}{\dot{D}_o B}\right) \qquad [39]$$

The process involves determining both B and mx iteratively since both are unknowns.

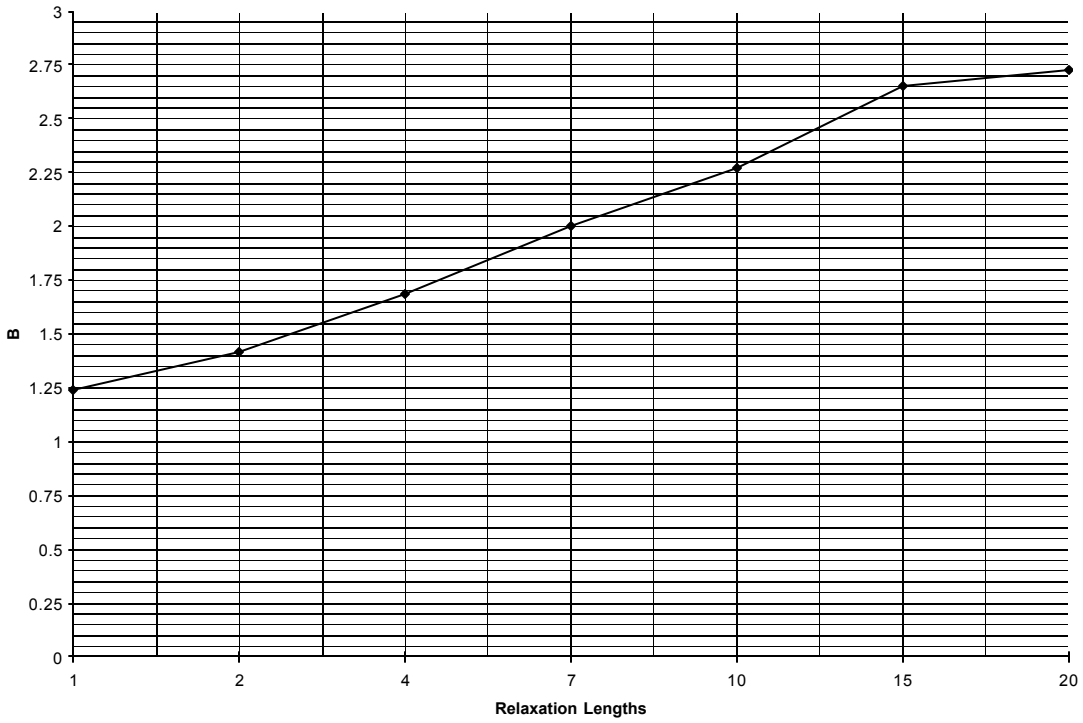

Figure 7. Buildup Factor vs. Relaxation Lengths (40)

A guessed value of B is input into Eq. [39] and varied until the calculated value of the relaxation length the value for B match as shown in Fig. 7. Lead was chosen as the shield material in this study. It is likely that the cost of producing lead shields would be less than some of the other metals considered in this study, but it may not be the best option for an actual design based on its low melting temperature.

Invariably the most important value to determine is the shield loading (measured in kg/m^2) which allows one to calculate the shield mass knowing only the surface area of the shield. Shield loading is obtained by multiplying the shield thickness by the density of the shielding material. An important point to make here is that this analysis is valid only for a monodirectional beam normally incident on a slab shield (36:553) since the buildup factors used were generated specifically for such an application. Shields of various different shapes can use the same method but require different buildup factors. Consider also that $^{178}Hf^{m2}$ is not a source for a monodirectional beam of gamma-radiation when viewing these results. The hope is that the worst case scenario is captured by assuming the emission of 600 keV photons, where in reality; the photons released will range between 12.7 and 574-keV (see Fig. 1).

Table 23 in Appendix E shows the trends established in this study of shielding a gamma-ray source. Quantities such as the distance from the source (r), the allowable dose rate ($\dot{D}$), the distance between the shield and the source, and the percentage of power radiated to the surroundings were varied for a constant area shield to determine their affects on shield thickness, loading, and ultimately mass. The vales shown in Appendix E are generic and not specifically associated with any of the core designs in this study. These examples were merely carried out to gain an understanding of shield

placement and the variation of shield weights that could be expected in the actual designs.

3.7. Individual Reactor Design for Fission and Isomer Cores.

The process of designing a TIC will look first at the materials that would be the best candidates to make up the core based on their history of use in such an application, material properties, and material interaction with electromagnetic radiation. Choice of a particular core configuration depends on mission requirements, heat transfer capabilities, necessary alteration, and manufacturability. The TIC core concept was applied only to the PBR design.

3.7.1. NERVA. The NERVA design, as discussed early, incorporates approximately 300 hexagonally shaped fuel elements with the uranium fuel dispersed in a variety of manners within a graphite matrix (3:452). The rate of fission within the core is controlled by rotary drums in the radial reflector region of the reactor and coolant channels run through the fuel elements to cool the reactor. An analysis of replacing the uranium fuel particles with $^{178}Hf^{m2}$ was not possible in this study, nor recommended. Little detail was found regarding the arrangement of the fuel within the graphite matrix, and realistic estimates of the achievable temperatures in this type of design are not possible for a TIC at this time. The maximum temperature achieved in the NERVA test series was 2,361 K (3:457) since the configuration used is not the one best suited for heat transfer. Materials used in the NERVA core had melting temperatures well above 3,000 K (Table 11). Specific sizing equations were not available without an in depth analysis (3:476) of the

fission process, and that was deemed unnecessary here. Instead, in the case of the fission design the core volume (V_{core}) and mass (m_{core}) were estimated by using quantities such as the power required (P_{req}) and power density (P_{den}) of the core.

$$V_{core} = \frac{P_{req}}{P_{den}} \quad [40]$$

$$m_{core} = \rho_{core} * V_{core} \quad [41]$$

3.7.2 CERMET. The CERMET design is similar to the NERVA reactor in that hexagonal shaped fuel elements with straight coolant channels were utilized. Other than differing on the principal of fast fission, the CERMET design also utilized uranium fuel particles embedded in a metal matrix. In addition to the uranium fuel the matrix materials consisted of molybdenum, tungsten, and rhenium. Both tungsten and rhenium have melting temperatures on par with the carbide compounds used in many reactor designs, and are also both very good attenuators of gamma-rays. As with the NERVA design, surface area for heat transfer is not maximized in this design resulting in a reactor that would not live up to the true potential of the heat generated within it. For the fission reactor design there are linear, least-squares curve fits for their CERMET sizing (3:489).

$$R_{core} = 0.0034 P_{req} + 20.79 \quad [42]$$

$$H_{core} = 0.0067 P_{req} + 41.418 \quad [43]$$

These were used to estimate the core dimensions for a fission core. The core volume (V_{core}) was then obtained with the equation $V_{core} = \pi R_{core}^2 * H_{core}$ and the core density (ρ_{core}) can be used to calculate the core mass (m_{core}) by the equation $m_{core} = \rho_{core} * V_{core}$.

3.7.3. Particle-Bed Reactor. The unique nature of the PBR design allowed for a closer look at the heat transfer taking place within the core, and the method employed (3:491) starts with the analysis of a single pellet. Assuming that some of the pellets are hafnium isomer and some are another metal suitable to absorbing the energy given off by the isomer, and knowing the maximum propellant temperature achieved in the core, the temperature at the pellet-coating interface can be determined making the following assumptions.

1. Every pellet is surrounded by a protective layer of zirconium carbide with a thickness of 1 μm.
2. Steady state heat generation and removal can be achieved. This results in a steady state process where the energy of the photons released during the decay is absorbed in the core materials, conducted to the materials outer surface (in this case the pellet's outer surface), and finally transferred to the propellant by convective heating.
3. The spectrum of photons released contains or generates trigger photons within the core will trigger the decay of additional atoms of the isomer.
4. The flow speed through the reactor is low enough to allow boundary layer effects at the pellets outer surface to be neglected. Subsequently there is not a large temperature difference between the temperature of the propellant at the location of maximum temperature within the core and the temperature of the pellet's outer surface.

The equation governing conduction used in this process is derived from Fourier's law for conduction and applied to the spherical pellets of the design.

$$\dot{Q}_x = -kA\frac{\Delta T}{\Delta x} \qquad [44]$$

For metals needing protection from the flow of fuel the coating of the pellets used in this study was assumed to be made up entirely of zirconium carbide (ZrC), but in actuality there are likely a couple of thin layers of graphite separating the zirconium carbide from the inner material. Though important for actual design the impact of this is assumed to be negligible in the heat transfer analysis conducted here. The pellet size was set by assuming a pellet inner diameter of 300 microns (hafnium isomer or other material) and an outer diameter of 500 microns which includes the layers of protective coating. Knowing this both the pellets outer surface area (represented by A in Eq. [44]) and the pellet volume can be determined. An approximation was made that 88% (3:491) of the volume occupied by a bed of pellets is actually the pellets with the remaining 12% being the voids between pellets.

The process began with setting the desired propellant temperature to 2,400 K. This is below the melting point of hafnium, a necessity of this design if metallic hafnium is used, and far enough below this melting point to allow the hafnium isomer to exceed this temperature without melting. In the instance that hafnium carbide can be used the propellant temperature is escalated to 3,500 K in this study, since higher values would exceed the limits of the specific heat equations being utilized. From this the power necessary to achieve these temperatures can be obtained, as well as the rocket performance characteristics such as specific impulse, the initial mass savings, and overall

mission feasibility (Sec. 3.3.5). This calculated core power requirement for heating was applied to two hypothetical reactor efficiencies (82% and 67%), to simulate the power lost from the core. The efficiency of 82% is based on the data provided for the PBR (Table 1) and its calculation is shown in Appendix H (H.1). The value of 67% was used to show the affect of decreased efficiency on core mass. Knowing the power requirement (P_{req}) allows for determining the reactor dimensions using Eqs. [45] and [46] (3:487) shown below. These two equations calculate the radius and height, respectively, of a 19-element PBR. Equations for two other possible configurations are displayed in Appendix D. Different reactor dimensions and masses result from each configuration, and a choice is made usually to select the lightest reactor, taking into account that the smallest radial dimension will also lead to a less shadow shield requirement.

$$R_{core} = -2.655(10)^{-12} P_{req}^5 + 8.946(10)^{-9} P_{req}^4 - 1.1703(10)^{-5} P_{req}^3 + 7.427(10)^{-3} P_{req}^2 - 2.2955 P_{req} + 313.34 \quad [45]$$

$$H_{core} = -4.027(10)^{-5} P_{req}^2 + 0.1427 P_{req} + 17.9883 \quad [46]$$

Knowing core radius and height one simply needs to apply the relations shown earlier (Sec. 3.7.2) to compute core volume and mass. For TIC application this mass value does not accurately represent the changes that will need to occur in this design.

The fission design of the PBR as described earlier (see Sec. 2.3.3) when applied as a TIC design would no longer require the moderator blocks to be of a material suitable for slowing down neutrons produced during fission. The material that is used for the pellets in the bed should also be changed. While the hafnium isomer will be present in the form of some of these pellets, in a quantity that will be set by the needs of the system, the remainder of these pellets can be constructed of another material possessing the

desired properties. A TIC should consider using materials that are good attenuators of photons and possibly producers of trigger photons as a result of the gamma-radiation initially absorbed. The original designs have core densities around 1,600 kg/m^3 (3:490). Deduced from a calculated core volume, the densities of uranium-carbide, zirconium-carbide, and beryllium, and values for the pellet size was the following fractional break up of the core; 8% of the core by volume is fuel pellets with coating, 58% of the core is moderator material, and the remainder is flow passages for the propellant and spacing. Of the 8% that is pellets, 21.6% of this volume is actual fuel, with the remaining 78.4% being coating material. Appendix H (H.3) displays these calculations which are based on the recommendation of 1/3rd of the core by mass being fuel pellets and their coating with the remaining two-thirds being moderator (34). With these values a mass estimate for a core altered for isomer decay can be obtained replacing materials as desired.

The number of pellets (N_p) within the core will determine how much power is available per pellet in this analysis. This is determined by dividing the mass of the fuel in the core by the mass of an individual fuel pellet.

$$N_p = \frac{r_{xx}(0.08)(0.216)V_{core}}{m_{pellet}} \qquad [47]$$

The power absorbed and available for heating the propellant was then calculated by

$$\dot{Q}_x = \frac{P_{req}}{N_p} \qquad [48]$$

Rearranging Eq. [44] then yields

$$T_s = T + \frac{\dot{Q}_x \Delta x}{kA} \qquad [49]$$

For the case of metallic hafnium, the propellant temperature T is set at 2,400 K and the temperature of the fuel pellets surface area is calculated. The value of the thermal conductivity was varied to view the impact on energy transfer since thermal conductivity values could change in the instance that other materials are used (Appendix H (H.4.2)).

4. Results

4.1 Propellants. The performance requirements for a rocket engine in this study were set by the need to perform the missions of the 1st and 2nd stages of the Delta IV-H (Table 2). The first step taken in this process was to verify what propellants would be suitable to carry out these missions in a monopropellant reactor design. Each nuclear core (NERVA, CERMET, and PBR) was examined with various propellants (Table 7) and judged on the basis of: its ability to perform the mission (Eq. [28]), the mass of propellant required for the mission (Eq. [25]), and the potential for thermal choking (Eq. [31]).

Table 7. Specific Impulse (I_{sp}) Values for Various Propellants

Engine	NERVA		CERMET		PBR	
Stage	1st	2nd	1st	2nd	1st	2nd
Temperature (K)	2,361		2,507		3,200	
Expansion Ratio	21.5	285	21.5	285	21.5	285
H_2	798	873	824	903	941	1037
CH_4	322	379	332	395	374	447
CO	216	234	223	244	252	277
CO_2	186	213	192	222	217	252
N_2	216	234	222	244	251	277
O_2	203	222	210	232	239	265
C_3H_8	269	265	281	282	330	331

In both cases hydrogen is the only propellant capable of performing the mission. This is no surprise considering that H_2 has the lowest molecular weight. This leads to higher values of specific impulse and exhaust velocity than heavier propellants. Methane (CH_4) was the one other propellant possessing a specific impulse value near that of the chemical rocket; calculated to be 447 s in a 2nd stage PBR design. There would be little value in its utilization, since reactor masses and the necessity of shielding would likely increase the overall rocket mass without a reduction in fuel usage. Even for propellant temperatures above 3,200 K, specific impulse values for the other propellants do not increase significantly, and there is no promise, for an application such as this, in the other propellants studied here. Figure 8 shows the specific impulse variation as a function of temperature for a 2nd stage PBR with a nozzle expansion ratio of 285:1. These values were calculated with the method described in Sec. 3.3.1.

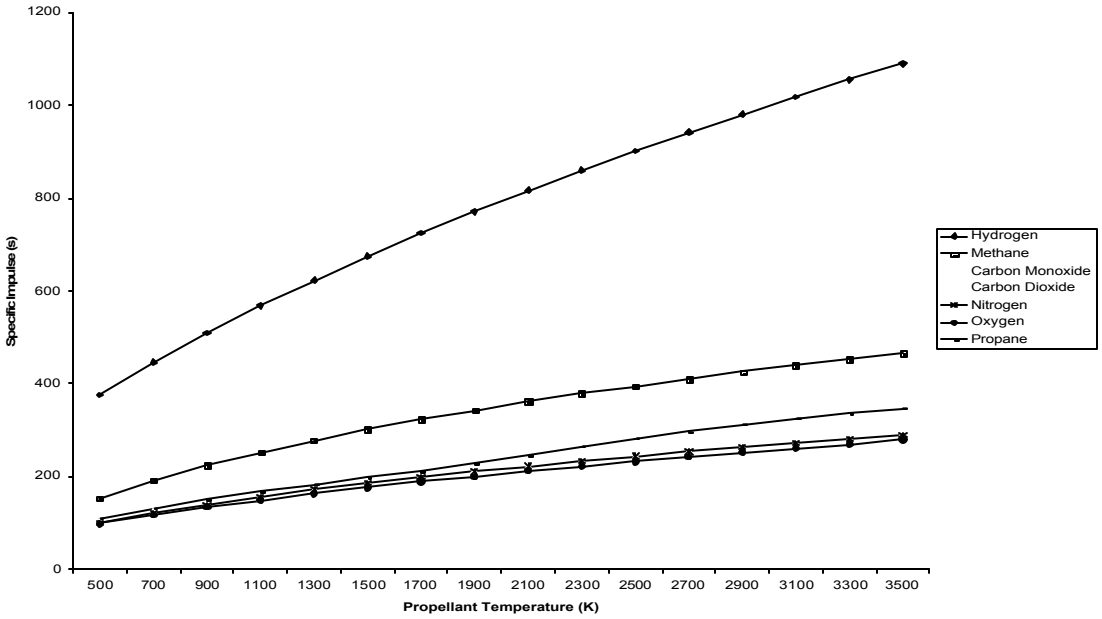

Figure 8. I_{sp} variation with temperature

The performance that results from using H_2 will be examined in Sections 4.2 and 4.3, but the choice of H_2 as a rocket systems propellant brings along some important engineering considerations. In order to store hydrogen onboard a spacecraft it must be cooled to its liquid state at 20.39 K, which requires special attention to the coolant storage and transportation system within the rocket. On a thermal rocket this means that heat from the reactive core must be prevented from raising the temperature of the propellant prior to its release from the storage tank. In both stages of the Delta IV-H considered here, cryogenic hydrogen is already utilized proving that storage issues can be handled, yet the possibility that escaping radiation could prematurely heat the propellant must be given some thought during shielding design. Also, metallic hafnium, proposed to be the source of energy in this system, rapidly absorbs hydrogen at temperatures around 973 K to form the compound HfH (50). If the isomer can produced in the form of hafnium carbide (HfC), this will cease to be a concern.

There may be potential in some other light propellants not considered here, but for the purpose of addressing the design of a TIC and making comparisons against fission reactors, the choice of hydrogen is made. Further time could be invested in the performance and properties of hydrogen at the operating temperatures achieved, but this should not be a large concern during preliminary design since the fission reactors tested in the past made use of this propellant (3:457; 5).

4.2 Analysis of Stage 1.

The nuclear fission reactors examined (NERVA, PBR, and CERMET) all vary with respect to their abilities to achieve high propellant temperatures and maintain high

values of chamber pressure throughout the reactor. Included here are the thermal efficiencies, some probable values of the core densities (3:490) and power densities. The achievable power density of the CERMET reactor was not found, but is said to be the highest of all the reactors due to the absence of moderator material (3:489). See Appendix H (H.1) for the calculation of these efficiencies.

Table 8. Nuclear Core Approximations

Reactor	**Thermal Efficiency**	**Core Density (kg/m^3)**	**Power Density (GW/m^3)**
NERVA	83%*	2,300	1.57
CERMET	90%*	8,500	> 40 (variable)
PBR	82%*	1,600	40 (variable)

Shown in Table 9 are the performance values of the three nuclear fission designs in a scenario replacing the 3 RS-68 engines on the Delta IV-H with a nuclear heat source. As stated earlier the specifics of the system design are not the focus of this study and the chamber pressure and its effect on system mass and performance will not be examined here, beyond noting that the lower chamber pressures will lead to lighter pressure vessels and larger nozzle dimensions for these nuclear designs (Sec. 3.3.4). The values listed are indicative of what can be achieved with these reactors, but in no way are meant to represent the limitations of these designs. The specific impulse values for each fission reactor listed in Table 9 are those generated in this study, with the nozzle expansion ratio of the Delta IV-H systems, along side those that are obtained from Table 1 (3:457) which are denoted by the asterisk.

Table 9. 1st Stage Nuclear Performance Comparison.

Engine	RS-68 (22)	NERVA		CERMET		PBR	
Propellant	LOX/LH_2	LH_2		LH_2		LH_2	
Chamber Pressure (MPa)	9.21	6.89		4.14		6.18	
Specific Impulse (s)	420	798	825*	824	930*	941	971*
Propellant Required (kg)	598,800	420,360		412,380		380,210	
$\dot{m}$ **(kg/s)**	Varies	1,270		1,229		1,077	
Power (MW)	-	41,794		43,623		51,832	
Engine Mass (kg)	~6,604 each {3} (51)	61,227		-		-	
Engine Volume (m^3)	?	26.62		-		-	
Full Shield Mass (kg)	-	>144,289		-		-	
F/W	1.4	<1.39		-		-	
Mass Savings (kg)	-	-7,314		-		-	

Propellant requirements for all of the nuclear designs drop off appreciably due to the increased values of specific impulse available. As a check of the specific impulse values calculated the specific impulse was also determined in this work using the documented expansion ratios only varied from the tabulated data on average by 4%. Appendix H (H.2) displays the manner in which specific impulse can be obtained utilizing the procedure described in Sec. 3.3.1.

A significant issue manifests when one tries to estimate the size of a reactor needed to provide a thrust sufficient to launch a vehicle of this magnitude into space.

The sizing estimates based on reactor power (Sec. 3.7) for the CERMET and PBR reactors don't apply for power requirements above a few thousand megawatts, and in order for the power requirements of an individual reactor to be this low; at the fewest 15 CERMET reactors or 26 PBR (of the 37 element configuration) would be needed. These numbers were obtained by dividing the core powers listed in Table 9 by 3,000 MW and 2000 MW respectively. This would likely never be considered as an option regardless of the source of heat energy due to shear complexity. Therefore, values for a CERMET and PBR engine and shield were not calculated for this stage. The mass and volume of a NERVA engine can be approximated for this application via the method described in Sec. 3.7 and is displayed in Appendix H (H.5), and it can be shown that to perform this mission with one engine it would have to be approximately 26.6 m^3 in volume and weight 61,226 kg. This is assuming that it operates with 100% efficiency at the established power density of 1,570 MW/m^3. If the linear trend, provided up through values of 2,000 MW (3:489), holds for NERVA reactors of much greater power levels then these values should be accurate to within a few percent.

Shielding necessary to provide protection against the radiation being released was based on the shield loading factor of 3,500 kg/m^2 and an approximated shield surface area of 41 m^2 (approximating the reactor height to be twice the value of the radius). In actuality the shield surface area would likely be larger as this value is a probable surface area of the reactor itself, and the shield loading would most likely increase since the power levels considered here are many times larger than those of the reactor designs. This proposed shield would surround the cylindrical reactor concentrically and on top,

resulting in a shield mass greater than 144,289 kg offsetting the benefits of the high specific impulse value obtained.

During such a 1st stage ascent, a rocket using $^{178}Hf^{m2}$ as the source of energy would require somewhere between 11 and 14 kg of the isomer to undergo decay, not to mention the additional hafnium needed in the configuration to maintain the chain reaction throughout the ascent. The equations of Sec. 3.4 were used to obtain these values. At the estimated near term rate of production (100 g/yr) it would take 140 years to produce this much hafnium isomer. For this reason alone it would not be prudent to consider further the construction of a TIC for such high thrust missions, not to mention of the material cost. No cost figures were determined in this study, but the price is certain to be high due to its limited availability and the nature of the process through which it is obtained. The method described in Sec. 3.6.2 cannot be used to estimate shield thickness or shield loading factor for power levels as high as predicted here. The level of radiation released extends beyond the data that supports this study (Fig. 7). Dense materials are needed for the attenuation of gamma-rays, and shield loading factors will be greater than those obtained in the following analysis of stage 2 which are in the region of 1,300 to 1,400 kg/m^2. Once again there will be a large impact on the weight savings earned with high specific impulse values, and Fig. 9 shows that the choice to not include shielding would not be a smart one. A source operating at giga-watt power levels and only radiating 5% of the energy generated would result in exposure rate as high as 17 rad/s at 1,609 m (one mile) from the source. At this rate subtle effects of radiation could be detected in people after just a few seconds of exposure (Table 6), and this would not be acceptable by today's standards of safety. Dose is shown in a log scale in Fig. 9, for two levels of

radiation release, showing how dose with distance from the source falls off according to the inverse square law ($1/r^2$).

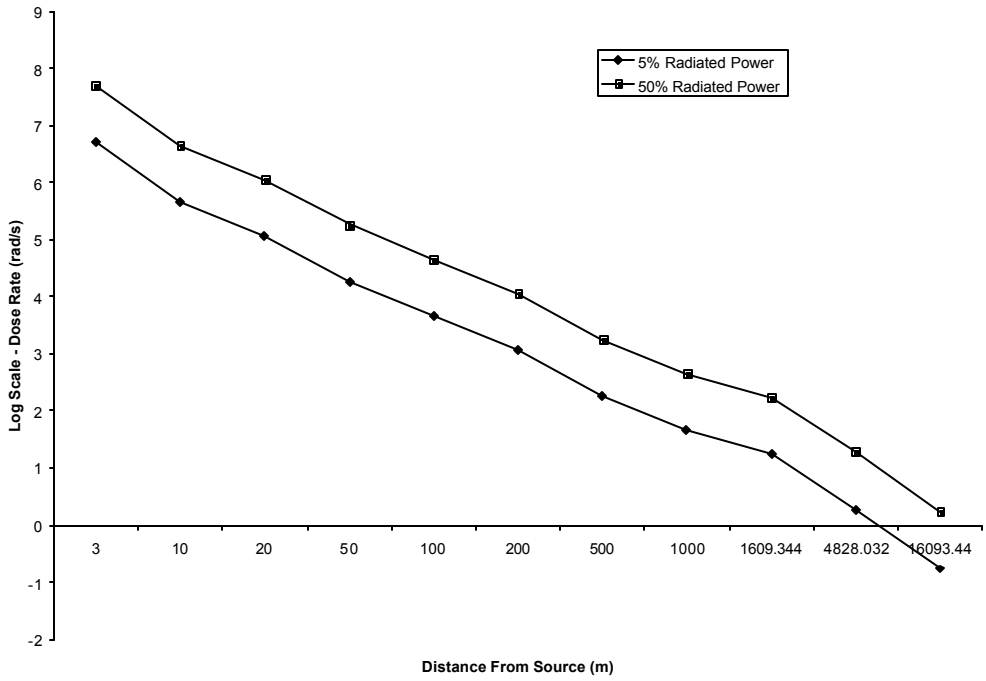

Figure 9. Radiation Dose vs. Distance

4.3 Analysis of Stage 2.

Estimates of engine mass and volume are now obtainable for all of the fission core designs since the core power levels required for this mission fall within the effective range of the equations used (Eqs. [42], [43], [45], and [46]). These estimates are displayed in Table 10 below. The calculations are carried out in Appendix H (H.2, H.5, and H.6) for the various core designs. Fission shielding was discussed in Sec. 3.6.1 and individual core design in Sec. 3.7.

For the 2nd stage application all three of the fission reactor designs are predicted to result in a significant mass savings over the chemical system used today. One major advantage that would result from applying nuclear technology to a mission such as this would be the ability to place shielding only between the spacecraft and the reactor itself, since radiation sent out into the space environment is of little concern. Of course this may raise issues if the spacecraft is to be used near other spacecraft, satellites, or space stations, since shield weights will escalate as the surface area requirement grows.

Table 10. 2nd Stage Nuclear Performance Comparisons

Engine	RL10B-2 (22)	NERVA		CERMET		PBR (19-element)	
Propellant	LOX/LH_2	LH_2		LH_2		LH_2	
Chamber Pressure (MPa)	3.21	6.89		4.14		6.18	
Specific Impulse (s)	462.4	873	825*	903	930*	1,037	971*
Propellant Required (kg)	26,529	17,310		16,870		15,162	
$\dot{m}$ **(kg/s)**	24.24	12.84		12.41		10.82	
Power (MW)	-	502		483		629	
Engine Mass (kg)	~ 277 (52)	736		600		547	
Engine Volume (m^3)	?	0.32		0.0706		0.342	
Shadow Shield Mass (kg)	-	1,511		553		1,303	
Vehicle *F/W* (including shield)	0.27	0.35		0.35		0.37	
Engine *F/W* (including shield)	40.5	5.0		9.7		6.1	
Mass Savings (kg)	-	7,249		8,783		9,794	

The rocket mass and velocity requirements of this type of mission appear to be the area where a nuclear source or TIC could have the largest impact and would be best suited to be introduced. The 2nd stage mission has a much lower thrust requirement (110,000 N), which is less than the documented capabilities of the original reactor designs (Table 1). It is very important to show that these designs can achieve the indicated propellant temperature, at this level of thrust. According to the data provided in Table 1, the PBR design is capable of exhaust velocities of 9,526 m/s (Eq. [16]) and propellant temperatures of 3,200 K. This results in a mass flow rate of 35 kg/s in order to achieve the documented 333,617 N of thrust (Eq. [15]). Mass flow rates for the PBR on this mission are around 10.82 kg/s (comparing values in Table 1 and Table 10), thus the determination is made the propellant temperatures assumed at the exit are indeed achievable.

Environmental concerns are minimized because the core could be kept inactive at low altitudes, and the short nature of the mission would guarantee that such a system could be tested for its length of operation in space on the ground prior to space flight. A mishap during launch would also not generate the radioactive particles that result in long lasting contaminants at the crash site, making this a safer choice than a fission reactor.

The minimum quantities of $^{178}Hf^{m2}$ needed to supply the energy for this mission (as determined by the method in Sec. 3.4) are also much less, ranging from 432 to 555 grams, for the various reactor designs. Production rates, while still not sufficient, would not have to improve much over current goals for this to be a near term reality. The importance of this is that if production goals of 100g/yr are reached, then the amounts of

hafnium isomer needed to perform these types of missions could be attainable within 4-5 years.

4.4 Designing the TIC.

With the basics laid for the level of improvement that can be expected for the 2nd stage mission by making the change to a fission based power source, we can now begin to put together the specifications for a TIC and estimate its level of performance. The operating principals for a TIC would be much the same as for the fission designs considered here, hence their importance to this work. The propellant needs to be heated to temperatures as high as possible, such that the maximum specific impulse values can be obtained. This will take place by having the propellant flow through a core of materials that serve the purposes of releasing energy, absorbing energy, providing protection to other materials, providing shielding for the rocket or surroundings, and supporting the physical arrangement of the core itself.

4.4.1 Shielding a Gamma-Ray Producing Source. Table 23 in Appendix E contains the data generated in a series of calculations, for generic cases, varying the important factors of shield design. These factors are the radiated power, the distance of the shield from the source, the distance of the equipment from the source, and the allowable level of exposure for whatever material is being protected. As a result the analysis described in Sec. 3.6.2 leads to the following conclusions about shield design for this type of source. A sample calculation for a 19-Element TIC design at 82% efficiency is displayed in Appendix H (H.4.1).

1. The placement of the shield with respect to the source does not affect the level of exposure to the radiation. The shield can be placed as geometric constraints of the rocket design allow. For shielding that extends beyond the simple geometry of a shadow shield, such as a cylindrical design or spherical design, the shield should be as close to the source as allowable to reduce its size and weight. For this study a shield distance of 0.5 m was selected.

2. For a decreasing allowable exposure rate, to levels as low as 1 μrad/s, the values of the buildup factor and relaxation length were off the charts used in this study and only placing great distances between the source and the equipment (out to 50 m) reduced the values enough to permit computation. For manned and vehicles bearing sensitive equipment this could be a large issue since heavier shields will be required (reducing the mass savings). This is an area for further investigation.

3. Equipment placed farther from the source required less shielding due to the inverse squared law of radiation falloff (Fig. 9).

4. The increase in shield weight for a 50% efficient source as compared to a 95% efficient source was only 94 kg. This is the difference in the mass values in column 13 and column 1 of Table 23. The achievement of lower levels of core efficiency with increased losses to radiation is not a large concern for the shield design. This could be especially beneficial in the case that waste heat needs to be radiated from the core, with steady requirements for rocket protection.

4.4.2 Material Selection. Due to the conditions within the core and the nature of the electromagnetic radiation being released in the decay process of $^{178}Hf^{m2}$, careful

consideration needs to be given to the choice of materials used. Materials within the core, most importantly, must be resistant to high temperatures if any increases in performance are to be seen. They must also maintain good physical, thermal, and mechanical properties in a harsh environment of high pressures and temperatures for the period of time that the mission dictates. That internal environment will be somewhat different from a fission reactor since the presence of the highly ionizing radiation is absent, namely the alpha particles and neutrons. Instead of materials that moderate, reflect, and absorb neutrons, the TIC will need materials that are good absorbers of short wavelength electromagnetic radiation (gamma-rays). For the purpose of maintaining a steady-state reaction within the core, means for producing the necessary trigger photons is needed, and certain materials may possess the ability to satisfy this need through fluorescence. Every material within the core may not satisfy all these requirements, but the combination of these traits between the materials included is essential for the realization of this idea. The background discussion of the nuclear fission reactors in Sec. 2.3 mentions several materials that could be essential to a TIC design, and Table 11 lists those important properties for selecting those that would be the best candidates for the design. Metallic hafnium has a melting temperature of 2,506 K, and that temperature is a limiting factor in this core design should hafnium carbide not be attainable. Regardless, no materials with lower melting temperatures than 2,506 K were selected for inclusion in the core. The assignment of a low, medium, or high value to a material's level of photon absorption is simply a distinguisher for the materials researched in this study. Those with a high mark were the best attenuators examined in this study and so forth. Information for some elements/materials could not be found.

Table 11. Recommendation on Materials

Element	Use in Fission Reactor	Level of photon absorption	Potential source of trigger photons	Melting Temperature (K)
Be	Reflector	Low	?	1,560
C	Support/Ceramic Formation	Low	?	3,800
Al	Pressure Vessel	Low	No	933
B	Control Drums	Low	?	2,573
Zr	-	Low	No	2,128
ZrC	Protective Coating	?	?	3,813
Nb	-	Medium-Low	No	2,750
NbC	Protective Coating	?	?	4,033
Mo	Attenuation	Medium	No	2,896
Hf	Control Drums	Medium	Yes	2,506
HfC	-	?	?	4,173
Ta	-	High	Yes	3,290
W	Attenuation	High	Yes	3,683
Re	Attenuation	High	Yes	3,443
Os	-	High	Yes	3,323
Pt	-	High	Yes	2,041
Pb	-	Medium	Yes	643

The best absorbers of radiation at short wavelengths (x-rays and gamma-rays) appear to be the dense transition metals such as hafnium, tantalum, tungsten, rhenium, and the highly toxic metal osmium. Those materials in the shaded blocks are the most favored candidates for a TIC since they posses a combination of the desired thermal properties and can serve either to absorb radiation or fluoresce as a result of it. The category entitled "potential source of trigger photons" needs clarification at this time. The assignment of a "yes" or "no" in this column simply indicates whether or not x-ray transition energies were found for this element in the range of interest (9 to 13, ~40, and ~60 keV). The ability to maintain a chain reaction in the core without the aide of an external photon source would be of great value to this system. Materials have been identified that posses the desired melting temperature and attenuation properties, yet also have electron transition that produce photons of the energies viewed to trigger the decay of $^{178}Hf^{m2}$. The probabilities for these transitions have not been established in this study, and it is recognized that none of these materials may actual satisfy the requirements for this type of design.

4.4.3 Configuration Selection. The choice was made in this study to apply the properties of a TIC to the PBR design configuration. The requirements of the mission being that of an upper stage vehicle and the ability of the particle-bed design to transfer the greatest amount of heat to the propellant were heavy factors in this decision. Large surface areas are required for heating propellants such as (H_2, NH_3, and H_2O) to absorb heat directly from a reactor (53). It is also possible, based on the individual nature of the fuel particles in this design, to conduct a more thorough analysis of the heat transfer

taking place as discussed in Sec. 3.7. This provides a more realistic view of the relationship between propellant and fuel particle temperatures within the core. A detailed analysis of the heat transfer taking place in a design such as this taking into account local heat variation, and radiation is not needed at this time. When the triggering of nuclear spin isomers is finally proven and shown to be capable of maintaining a chain reaction such an analysis would definitely be required. If hafnium carbide is used this becomes a mute point for this analysis since the chosen temperature of 3,500 K is far below the melting temperature of that material.

As mentioned in Sec. 3.7.3 the thermal conductivity was varied to identify its effect on interior pellet temperature. The plot below shows that there is a minimum required thermal conductivity of the coating material if the desired propellant temperatures are to be reached without exceeding the melting temperature of the fuel pellet. The data supporting this plot has been tabulated in Appendix H (H.4.2).

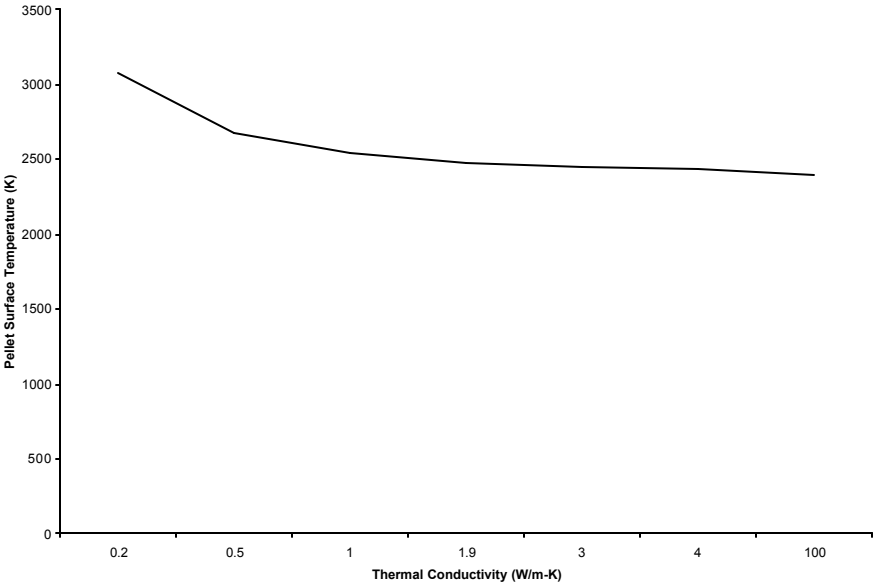

Figure 10. Effect of Thermal Conductivity on Propellant Temperature

Since the melting temperature for metallic hafnium is 2,506 K, coating material thermal conductivities should exceed a value of 1.0 W/m-K. The thermal conductivity of 1.9 W/m-K provided by Humble (3:492) for zirconium carbide coated pellets was used in this study.

With the choice of 2,400 K (metallic hafnium) and 3,500 K (hafnium carbide) as the desired static propellant temperature at the core outlet, the following values (Table 12) of specific impulse, minimum reactor power, and mass savings are achievable for this mission. The mass savings shown does not include the subtraction of the chemical engines mass, the addition of the TIC mass, or the required shielding. The method of Sec. 3.3.1, used for the fission core calculations (Appendix H (H.2.1 and H.2.2)), was also used to generate the values listed in Table 12. The flow geometry of the PBR is assumed to remain unchanged leading to chamber pressures no different from the fission core designs.

Table 12. First Iteration Core Properties

Propellant Temperature (K)	**Isp (s)**	**Minimum Core Power (MW)**	**Mass Savings (kg)**
2,400	881	422	9,340
3,500	1,090	548	11,960

For the case of the isomer in metallic form, realizing that 422 MW of power is needed to heat liquid H_2 to the desired temperature providing the required thrust of 110,000 N; two core efficiencies were examined to view the effect on the overall size of the core and the

shielding requirements. While the specifics of the core's arrangement was not examined in this study, it is understood that some of these pellets will be constructed of the hafnium isomer, and the total mass of isomer residing within the core will have to be adjusted depending on the amount needed to sustain a chain reaction at the desired rate. Sample calculations for metallic hafnium pellets are shown in Appendix H (H.4).

Table 13. Mass of Materials Replacing Pellets in a 19-Element PBR

Core Efficiency	82%	66.7%
Number of Pellets	392,610,596	418,157,176
Mass of Coating (kg)	136	144
Mass of Tungsten (kg)	104	111
Mass of Hafnium (kg)	74	79
Mass of Tantalum (kg)	92	98
Mass of Rhenium (kg)	117	124

As stated earlier only somewhere in the region of 432 to 555 grams of isomer would be need to undergo decay to supply the energy for this mission, so conceivably the percentage of pellets within the core that are constructed of the isomer could be very small. It is also conceivable that the remainder of the pellets making up the core could be a mixture of materials, but the results shown in Table 13 are rough estimates of the total pellet mass if a majority of the pellets are any one of the materials listed. Including hafnium in this list assumes that pure metallic form of the element in a non-excited state is being utilized in addition to the isomer. The coating composition was not varied in this study and its mass remains the same regardless of the material used.

Table 14. Mass of Materials Replacing Moderator in a 19-Element PBR

Core Efficiency	82%	66.7%
Core Volume (m^3)	0.3212	0.3421
Mass of Tungsten (kg)	3,506	3,734
Mass of Hafnium (kg)	2,480	2,641
Mass of Tantalum (kg)	3,102	3,304
Mass of Rhenium (kg)	3,916	4,171

The replacement of the moderator within the core with materials that were identified as the best absorbers of high energy electromagnetic radiation and as possible sources of the desired fluorescence will lead to much heavier core designs than those predicted by using a typical PBR core density. The densities of neutron absorbing material such as beryllium and lithium hydride are much less than those of the metals shown in Table 14. A sample calculation is shown in the beginning of Appendix H (H.4).

In the search for lighter elements possessing the desired properties stated above, no elements were identified as potential sources of the desired photon emission with melting temperatures even approaching 2,000 K. Provided a source for photon emission can be found amongst the heavier elements, the designer will be faced with the challenge of exposing the isomer to these photons before they are absorbed within the material that produces them (34).

A shadow shield constructed of lead and placed 0.5 m from the core, with allowable levels of exposure on the back side set at 0.01 rad/s, will result in the shield

masses shown in Table 15 for two different levels of core efficiency. As shown by the small masses calculated below the ability to simply use shadow shields is of great benefit a core designed for 2nd stage applications. Appendix H (H.4.1) contains the calculations for the 82% efficiency case.

Table 15. Shadow Shielding a 19-Element TIC-PBR

Radiated Power	Core Radius (m)	Tolerable Dose Rate (rad/s)	Shield Thickness (kg)	Shield Loading (kg/m^2)	Shield Mass (kg)
18%	0.3558	0.01	0.1208	1,377	548
33%	0.3428	0.01	0.1263	1,440	535

In this instance the shield mass is actually less for the lower efficiency case, but this is due solely to the fact that the increase in core power to account for the radiation losses has resulted in a core with smaller radial dimensions lessening the shadow shield are. According to the conduction law applied (Eq. [44]) and the assumption of an equal distribution of the energy released from the isomer within the packed bed, the melting temperature of metallic hafnium, and of course tungsten, will not be exceeded in this design. This is a very simplified analysis; however, assuming that the core as it is designed would result in such heat flow behavior. In actuality, the system would need to be modeled at a very detailed level in coordination with the actual core design. Presuming that a chain reaction can be initiated, much higher power densities could be achieved within the core, with effective heat removal governing the design (34). For this mission, however, a core power density similar to that shown in Table 16 would be sufficient, and the amount of hafnium isomer required to supply this power will be a

function of its susceptibility to triggering and the trigger photons production within the core.

Table 16. Actual Core Attributes for the 2,400 K Case

Core Efficiency	Total Core Power (MW)	Power Density (GW/m^3)	Pellet Core Temperature (K)	Power Absorbed / Pellet (W)
82%	443	1.602	2,472	1.075
66.7%	633	1.850	2,468	1.009

As a final comparison, probable TIC designs, utilizing a configuration similar to that of the 82% efficient, 19-element PBR design, are examined next to provide a comparison with the data tabulated on the NERVA, CERMET, and 19-element PBR fission reactor designs and RL10B-2 (Table 10). The TIC as shown is of three different constructions. One consists of replacing the pellets and moderator material of the fission design with all metallic hafnium, and hafnium isomer pellets are dispersed throughout the bed as needed. This would be the lightest TIC configuration. The other two replace the pellets and moderator material with the metal tungsten and hafnium carbide. The fact that some of the pellets within the tungsten design will actually be hafnium should not impact the mass estimates by much since both hafnium and hafnium carbide are less dense than tungsten. Also note that the hafnium carbide case is capable of higher core temperatures. All of the new core designs result in a level of improvement over the baseline system making a strong argument for their place as space propulsion options. Provided shadow shields can support the mission and the equipment on board is hardened

to radiation exposure levels of 0.01 rad/s, very significant mass savings can be achieved with any design as shown in Table 17.

Table 17. 2nd Stage TIC Mass Comparisons

Core Composition	Metallic Hf TIC	Tungsten TIC	Hafnium Carbide TIC
Specific Impulse (s)	881	881	1,090
Propellant Required (kg)	17,189	17,189	14,569
Power (MW)	515	515	668
Engine Mass (kg)	2,689	3,746	2,691
Engine Volume (m^3)	0.3212	0.3212	0.3342
Shadow Shield Mass (kg)	548	548	460
Vehicle *(F/W)*	0.31	0.31	0.35
Engine *F/W*	3.46	2.61	3.56
Mass Savings (kg)	6,380	5,323	9,086

A few notes on these numbers. The core masses have been calculated based on core sizes predicted for a fission reaction. The amount needed will depend heavily on the level of gamma absorption required for heating and the mass numbers calculated in the analysis shown in Appendix I for high levels of efficiency, suggest that these masses could be less. Secondly, the thrust-to-weight values are not maximum values since increases in propellant will allow for increases in mass flow rate, and increases in thrust for the same core weight. The vehicle thrust-to-weight (*F/W*) has been calculated by setting the new vehicle weight to a value equal to the original vehicle mass minus the mass savings. The manner in which this savings is applied is up to the user and the type of mission required.

The choice can be made of carrying near the current system's fuel load to increase the velocity change capabilities of the rocket. More Δv can mean faster transit times, further range in space, longer duration missions, or increases in the number or type of maneuvers carried out by the spacecraft. Durability of spacecraft could also be improved with the additional weight being used to design more rugged components, better shielding from the space environment, and systems capable of being used for longer periods of time. Due to the launch costs of today, the most important benefit of such a system would be the increase in payload mass that can be put into space. With a PBR design relying on isomer decay from a hafnium carbide core an additional 9,086 kg can be boosted into space. This would nearly double the payload limit for the current mission. Satellites tend to weigh from a few hundred to a few thousand kilograms (22:107-110), so if the payload bay can accommodate it and the fuel economy will allow it the number of satellites placed into orbit by this single vehicle could help reduce the number of launches need for placement of our space assets. With planned missions to the moon and requirements for construction in space (8), such as with the international space station, boosting greater payloads weights into orbit is of vital importance in the near future.

5. Conclusions and Recommendations

In this study three nuclear fission reactors and a conceptual core dependent on triggered isomer decay were examined in the role of providing thrust for the 1st and 2nd stages of the Delta IV-H rocket vehicle. The Delta IV-H, as designed, is dependent on chemical combustion resulting in specific impulse values for its 1st stage engine (the RS-68) of 420 s and for its 2nd stage engine (the RL10B-2) of 462.4 s. The goal was to identify increases in performance possible with alternative power sources taking into account the likely increase in engine mass due to the inclusion of shielding and changes in materials. Nuclear fission reactors have had to battle environmentalists and safety concerns over the course of their existence, leading scientists and engineers to look for propulsion sources capable of similar performance without the threat of harmful radioactive decay products. The isomer $^{178}Hf^{m2}$ is capable of high levels of energy storage (1.3 GJ/g), releasing only gamma-radiation during its decay. The absorption of gamma-radiation within materials can lead to the creation of charged particles, but does not lead to the formation of the long lived decay products common to the fission reaction. Based on the amount of energy stored, the length of time for which it is stored, and the resulting spectrum of decay, this material is viewed to have the potential for being a source of energy in space. This work examines the manner in which this material could be employed within a rocket to facilitate a chain reaction within the material and achieve the highest levels of heat transfer to a propellant. Due to its similarity to nuclear heat sources, the configurations examined were the NERVA, PBR, and CERMET.

5.1 Conclusions

1. Application of a nuclear or isomer core to a 1st stage rocket design will result in a significant reduction in the mass savings achieved by high levels of specific impulse. This is due to the requirement that shielding be placed around the entire core while active within the lower atmosphere. An isomer design without shielding will be dangerous to humans even at distances of miles from the source, and there is potential for radioactive decay products to be expelled in the rocket exhaust from fission core designs. The potential hazards outweigh the benefits of such a source for an application such as this since no fuel savings or increases in payload mass are predicted.

2. Based on reasonable weights for shadow shield designs, "light-weight" core designs, and increased levels of I_{sp}, achievable with hydrogen flowing through the fission designs, significant mass savings result for a Delta IV-H 2nd stage vehicle (Tables 10). Systems with such sources can capitalize on this savings by carrying more payload mass, achieving greater changes in velocity (Appendix F), traveling further into space, or becoming more rugged in design.

3. A PBR dependent on the fission of uranium-carbide fuel pellets can provide the mass savings as high as 9,800 kg when applied to the 2nd stage mission. Of the fission reactors examined in this study the PBR has the characteristics best suited to take full advantage of an isomer energy source. The particle bed reactor's pellets offer large surface areas for heat transfer, and the ability to manufacture the isomer pellets separate from the remainder of the core. Provided the pellets can be swapped out of the core, potential also exists for a reusable engine.

4. For the design of an isomer core in a particle bed configuration, high levels of efficiency can likely be obtained if core masses are increased to specifically absorb the spectrum of radiation being given off as a result of the decay. Absorbing gamma-radiation requires elements high in atomic mass and the core environment requires materials high in melting temperature. The isomer itself will have a melting temperature of 2,506 K in the metallic form, and a melting temperature of 4,173 K if hafnium carbide is used. The design dependent on triggered isomer decay for its energy would likely yield somewhat less of a mass savings (in the range of 6,000 to 9000 kg) due to increased material masses and lower melting temperatures (in the case of metallic hafnium), but such a design would benefit from the lighter shield mass needed to protect equipment from its spectrum of radiation when compared against a fission core. Shield loading factors for fission designs can be up to three times that of those for a gamma producing source alone (Appendix H).

5.2 Recommendations

1. While the triggering of $^{178}Hf^{m2}$ is still an area of active research, the investigation of photon emission from various materials could be the key to the successful application of this technology. Ultimately, achieving a chain reaction will depend on the sensitivity of the isomer to triggering, but equally important for applications such as this, are means for creating and maintaining the population of trigger photons within the core. The manner in which this is carried out is an area for continuing research.

2. The investigation of tailoring a PBR design to support the decay of the isomer, in addition to promoting a chain reaction within the included isomer material, should also include an analysis of the material quantities needed to effectively absorb the radiant energy within the core and the surface area requirements for convective heating. This will have a large impact on the core mass, which as estimated in this study, assumes a material configuration similar to that designed to support the fission reaction.

3. If high efficiencies are not obtainable as predicted by the estimates in Appendix I, or use is extended beyond unmanned mission, then shielding will become a more important aspect of this design. In order to examine weights for shield configurations other than that of a shadow shield, or with materials other than lead, build up factors specific to shield shape, type of source, and material are needed. Only a limited number of potential shield materials were listed in the sources used in this study, and further investigation in this area could lead to the optimization of shield designs for this application.

4. Though not an area of investigation in this thesis work, an argument can be made for all of these systems (nuclear and isomer) as sources of power for nuclear electric systems powering deep space mission. While the advantage of high specific impulse systems is more clear cut in the deep space mission category due to chemical systems inability to perform such missions, this does not mean that this is the best place for a system such as those considered here to make their first mark on the U.S. space program. Shorter missions such as orbit transfer, and possibly a trek to the moon would help prove the reliability of these systems and allow engineers to perfect their designs before traveling into the outer reaches of space on missions spanning decades. An isomer

core could even be returned home to study the effects of its operation in space, since radioactive decay products are not a concern with this type of energy source.

5. The isomer $^{178}Hf^{m2}$ is not the only material that releases energy in the form of high energy photons, such as gamma-rays. These sources of energy will require materials, such as those considered in this study, to capture the heat of the radiation if they are to be used for space propulsion applications. Should scientists be unable to release the energy stored in $^{178}Hf^{m2}$ reliably and on demand, then work such as this should be continued specific to more probable forms of energy generation.

Appendix A

Material properties are a very important to system design and sizing. Values for density (r), melting temperature (T_m), and thermal conductivity (k) at 300 K are listed.

Table 18. Element Properties

Element	Description	r (g/cm^3) (54)	T_m (K) (54)	k (W/cm-K) at 300K (55)
H	Hydrogen	0.08988	-	0.001815
Air	Main Group	0.001229	-	0.00024
Be	Alkaline Earth Metal	1.848	1560	2.01
LiH_2	Alkali & Hydrogen	0.500	962	0.0005-0.003
C	Main Group	2.267	3,800	1.290
Al	Main Group	2.700	933	2.37
B	Metalloid	2.3	2,573	0.274*
Ge	Metalloid	22.5	1,210	0.64
GaAr	Semiconductor	5.316*	1,510*	0.500
Zr	Transition Metal	6.511	2,128	0.227
ZrC	Ceramic	6.7*	3,813*	0.210*
Nb	Transition Metal	8.570	2,750	0.537
NbC	Ceramic	7.900*	4,033*	0.130*
Mo	Transition Metal	10.30	2,896	1.380
Sm	Lanthanide	7.353	1,345	0.133
Hf	Transition Metal	13.31	2,506	0.230
HfC	Ceramic	12.2	4,173	?
Ta	Transition Metal	16.65	3,290	0.575
TaC	Ceramic	15.00*	4,153*	0.220*
W	Transition Metal	18.82	3,683	1.740
WC	Ceramic	15.70*	3,143*	0.42
Re	Transition Metal	21.02	3,443	0.479
Pt	Transition Metal	21.09	2,041	0.716
Os	Transition Metal	22.5	3,323	0.9167
Pb	Main Group	11.37	643	0.353
U	Actinide	18.74	386	0.276
UC_2	Nuclear Fuel	11.3*	2,623*	3.3472
UC	Nuclear Fuel	13.5		2.3849 (avg.)
UO_2	Nuclear Fuel	10.97	2,827	0.270

* denotes items found on Matweb (56).

Appendix B

Table 19. Mass Attenuation Coefficient (μ/ρ) in cm^2/g

Gamma-ray Energy (keV)	10	100	200	300	400	500	600
H	0.3854	0.2944	0.2429	0.2112	0.1893	0.1729	0.1599
Air	5.120	0.1541	0.1233	0.1067	0.09549	0.08712	0.08055
Be	0.6466	0.1328	0.1089	0.0946	0.08471	0.07739	0.07155
LiH_2*	0.3449	0.1499	0.1234	0.1072	0.09603	0.08769	0.08111
C	2.373	0.1514	0.1229	0.1066	0.09546	0.08715	0.08058
Al	26.23	0.1704	0.1223	0.1042	0.09276	0.08445	0.07802
B	1.255	0.1391	0.1136	0.0986	0.08834	0.08065	0.07460
Ge	37.42	0.5550	0.1661	0.1131	0.09337	0.08212	0.07452
Ga	34.21	0.5197	0.1619	0.1123	0.09325	0.08236	0.07487
GaAr	37.80	0.5598	0.1671	0.1137	0.09371	0.08248	0.07484
Zr	74.17	0.9658	0.2237	0.1318	0.10180	0.08693	0.07756
Nb	80.38	1.0370	0.2344	0.1357	0.10400	0.08831	0.07858
Mo	85.76	1.0960	0.2423	0.1379	0.10470	0.08848	0.07851
Sm	249.9	2.9010	0.5192	0.2296	0.14660	0.11120	0.09218
Hf	230.1	4.1540	0.7339	0.3054	0.18340	0.13240	0.10580
Ta	237.9	4.3020	0.7598	0.3149	0.18810	0.13520	0.10760
W	96.91	4.4380	0.7844	0.3238	0.19250	0.13780	0.10930
Re	101.1	4.5870	0.8119	0.3339	0.19760	0.14090	0.11400
Os	104.5	4.6960	0.8327	0.3414	0.20110	0.14280	0.11250
Pt	113.2	4.9930	0.8896	0.3625	0.21180	0.14920	0.11680
Pb	130.6	5.5490	0.9985	0.4031	0.23230	0.16140	0.12480
U	179.1	1.9540	1.2980	0.5192	0.29220	0.19760	0.14900

* weighted average

Mass attenuation and mass energy absorption coefficients were obtained online at the National Institute of Standards and Technology (NIST) website (57). The gamma-ray

energies chosen where based on the spectrum of decay emitted from $^{178}Hf^{m2}$ which range from 12.7 to 574 keV in energy (Fig. 1). The materials listed in Tables 19 and 20 are current materials used in fission reactors, mediums through which the produced radiation will pass, or probably materials for constructing a TIC.

Table 20. Mass Absorption Coefficient (μ_A / ρ) in cm^2/g

Gamma-ray Energy (keV)	10	100	200	300	400	500	600
H	0.00985	0.04063	0.05254	0.05695	0.0586	0.059	0.05875
Air	4.742	0.02325	0.02672	0.02872	0.02949	0.02966	0.02953
Be	0.4225	0.01838	0.02353	0.02548	0.02620	0.02639	0.02627
LiH_2	0.1222	0.02066	0.02666	0.02889	0.02971	0.02991	0.02980
C	2.078	0.02147	0.02655	0.02870	0.02950	0.02969	0.02956
Al	25.43	0.03794	0.02745	0.02816	0.02862	0.02868	0.02851
B	1.006	0.0194	0.02453	0.02654	0.02731	0.02749	0.02737
Ge	35.64	0.3803	0.06865	0.03891	0.03193	0.02930	0.02790
Ga	32.50	0.34970	0.06463	0.03782	0.03156	0.02920	0.02793
GaAr	36.01	0.38380	0.06921	0.03916	0.03210	0.02943	0.02802
Zr	71.50	0.70800	0.11640	0.05420	0.03885	0.03311	0.03025
Nb	77.54	0.76080	0.12470	0.05705	0.04026	0.03396	0.03085
Mo	82.75	0.80420	0.13160	0.05919	0.04117	0.03437	0.03104
Sm	227.8	1.78600	0.33660	0.13260	0.07620	0.05411	0.04334
Hf	197.5	2.07500	0.46450	0.18530	0.10350	0.07044	0.05409
Ta	202.1	2.09200	0.47840	0.19150	0.10690	0.07248	0.05545
W	92.04	2.10000	0.49130	0.19730	0.11000	0.07440	0.05673
Re	96.10	2.10700	0.50540	0.20380	0.11350	0.07658	0.05822
Os	99.40	2.09200	0.51500	0.20850	0.16100	0.07813	0.05923
Pt	107.8	2.08100	0.54130	0.22160	0.12330	0.08265	0.06230
Pb	124.7	1.97600	0.58700	0.24550	0.13700	0.09128	0.06819
U	171.1	1.50200	0.67460	0.30500	0.17320	0.11520	0.08494

The expressions $1/m$ and $1/m_A$ represent the average distance traveled, measured in centimeters, before a photon respectively either interacts with or is absorbed in the material it is traversing. The shaded blocks indicate the materials which exhibit the best attenuation or energy absorption characteristic, and should be considered first as candidates for a TIC design. In order to get some idea of the distance a photon will travel through a material before either interacting or depositing its energy, the mean free path can be expressed as $1/m$ or $1/m_A$ measured in cm. This is an average distance value calculated for a couple of different energy photons as shown in Table 21.

Table 21. Mean Free Path for Attenuation and Energy Absorption

Photon Energy		**10-keV**		**300-keV**		**600-keV**	
Element	r **(g/cm^3)**	$1/m$ **(cm)**	$1/m_A$ **(cm)**	$1/m$ **(cm)**	$1/m_A$ **(cm)**	$1/m$ **(cm)**	$1/m_A$ **(cm)**
Hf	13.31	0.000327	0.000380	0.246	0.406	0.710	1.39
Ta	16.65	0.000252	0.000297	0.191	0.314	0.558	1.08
Pb	11.37	0.000673	0.000705	0.218	0.288	0.705	1.04
W	18.82	0.000548	0.000577	0.164	0.269	0.486	0.937
Re	21.02	0.000471	0.000495	0.142	0.233	0.417	0.817
Pt	21.09	0.000419	0.000440	0.131	0.214	0.406	0.761
Os	22.5	0.000425	0.000447	0.130	0.213	0.395	0.750
H_2	0.08988	28.9	1,130	52.63	200	6.944	189
Air	0.001229	159	172	7,626	28,331	10,101	27,554

Appendix C

Specific heat equations were obtained from two different sources. As shown below, the equations with inputs temperature (T) and the molecular mass (MM) of the gas will yield the specific heat value (c_p) of the indicated gas in J/kg-K.

From Humble, Henry, and Larson (3:460):

H_2: $$c_p = \frac{1000 J/kJ}{MM_{H_2} kg/kmol}[56.505 - 702.74(\frac{T}{100})^{-0.75} + 1165(\frac{T}{100})^{-1} - 560.7(\frac{T}{100})^{-1.5}] kJ/kmol-K$$

CH_4: $$c_p = \frac{1000 J/kJ}{MM_{CH_4} kg/kmol}[-67287 + 43974(\frac{T}{100})^{0.25} - 24875(\frac{T}{100})^{0.75} + 32388(\frac{T}{100})^{-0.5}] kJ/kmol-K$$

CO_2: $$c_p = \frac{1000 J/kJ}{MM_{CO_2} kg/kmol}[-3.7357 + 30.529(\frac{T}{100})^{0.5} - 4.1034(\frac{T}{100}) + 0.024198(\frac{T}{100})^2] kJ/kmol-K$$

From Chemkin data file (47). Value in brackets is unites and Ru is in J/kmol-K here only.

CO: $$c_p = \frac{Ru}{MM_{CO}}[3.025078 + 0.001442689T - 0.05630828x10^{-5}T^2 + 0.01018581x10^{-8}T^3 - 0.06910952x10^{-13}T^4]$$

N_2: $$c_p = \frac{Ru}{MM_{N_2}}[2.926640 + 0.0014487977T - 0.05684761x10^{-5}T^2 + 0.0109704x10^{-8}T^3 - 0.06753351x10^{-13}T^4]$$

O_2: $$c_p = \frac{Ru}{MM_{O_2}}[3.697578 + 0.0006135197T - 0.01258842x10^{-5}T^2 + 0.01775281x10^{-9}T^3 - 0.01136435x10^{-13}T^4]$$

C_3H_8: $$c_p = \frac{Ru}{MM_{C_3H_8}}[7.525217 + 0.01889034T - 0.06283924x10^{-4}T^2 + 0.09179373x10^{-8}T^3 - 0.04812410x10^{-12}T^4]$$

Appendix D

Particle-Bed Reactor sizing equations (3:486) were obtained for three reactor configurations (7, 19, and 37) which insure criticality in a fission reactor and geometrically fit together to form a nearly circular shape. The input to these equations is the desired core power (P_{req}) and the output is core radius (R_{core}) and core height (H_{core}).

For 7 Elements:

$$R_{core} = 9.0958(10)^{-10} P_{req}^4 - 1.3261(10)^{-6} P_{req}^3 + 7.1665(10)^{-4} P_{req}^2 - 0.1735 P_{req} + 47.625$$

$$H_{core} = -0.000283 P_{req}^2 + 0.5203 P_{req} + 26.06$$

For 19 Elements:

$$R_{core} = -2.655(10)^{-12} P_{req}^5 + 8.946(10)^{-9} P_{req}^4 - 1.1703(10)^{-5} P_{req}^3 + 7.427(10)^{-3} P_{req}^2 - 2.2955 P_{req} + 313.34$$

$$H_{core} = -4.027(10)^{-5} P_{req}^2 + 0.1427 P_{req} + 17.9883$$

For 37 Elements:

$$R_{core} = 4.905(10)^{-11} P_{req}^4 - 2.881(10)^{-7} P_{req}^3 + 6.2522(10)^{-4} P_{req}^2 - 0.5992 P_{req} + 252.28$$

$$H_{core} = -6.502(10)^{-6} P_{req}^2 + 0.05009 P_{req} + 18.335$$

Appendix E

Figure 9 in the text shows that radiation dose falls off according to the inverse square law ($1/r^2$), and the data in Table 22 was used to build that figure. The power being produced was for a 1st stage application and measured 41,794-MW. The cases of 5% and 50% of the produced power radiated were examined.

Table 22. Radiation Dose as a Function of Distance from the Source

Percent Radiated	**0.05 percent radiated**		**0.5 percent radiated**	
Distance (m)	**Dose rate (rad/s)**	**Log scale**	**Dose rate (rad/s)**	**Log scale**
3	4988800	6.697996094	49888000	7.697996094
10	448990	5.652236668	4489900	6.652236668
20	112250	5.05018635	1122500	6.05018635
50	17960	4.254306332	179600	5.254306332
100	4490	3.652246341	44899	4.652236668
200	1123	3.050379756	11225	4.05018635
500	180	2.255272505	1796	3.254306332
1000	45	1.653212514	450	2.653212514
1609.344	17	1.230448921	173	2.238046103
4828.032	1.9	0.278753601	19	1.278753601
16093.44	0.17	-0.769551079	1.7	0.230448921

Table 23. Shielding a Gamma-Ray Source

Radiated Power (MW)	20.6	20.6	20.6	20.6	20.6	20.6	20.6	20.6	20.6	206	412
Shield Distance (m)	0.5	2	3	0.5	0.5	0.5	0.5	0.5	0.5	0.5	0.5
Equip. Distance (m)	3	3	3	3	3	10	1	5	10	3	3
Equip. Tolerance (rad/s)	0.1	0.1	0.1	0.001	0.000001	0.000001	0.01	0.01	0.01	0.01	0.01
Intensity (W/m^2)	182,130	182,130	182,130	182,130	182,130	16,392	1,639,200	65,566	16,392	1,821,300	3,642,600
Dose (rad/s)	49,175	49,175	49,175	49,175	49,175	4,426	442,570	17,703	4,426	491,750	983,490
Dose Buildup Factor	2.66	2.66	2.66	2.71	Off Chart	Off Chart	2.7	2.67	2.45	2.71	2.72
Relaxation Length	16.39	16.39	16.39	18.70	Off Chart	Off Chart	18.60	15.37	13.90	18.71	19.40
Shield Thickness (m)	0.1106	0.1106	0.1106	0.1262	-	-	0.1255	0.1037	0.0938	0.1262	0.1309
Shield Loading (kg/m^2)	1260.84	1260.84	1260.84	1438.68	-	-	1430.70	1182.18	1069.32	1438.68	1492.26
Area (m^2)	.4062	.4062	.4062	.4062	.4062	.4062	.4062	.4062	.4062	.4062	.4062
Mass (kg)	512.15	512.15	512.15	584.39	-	-	581.15	480.20	434.36	584.39	606.16

Appendix F

Calculating the velocity change requirements for the two stages of the Delta IV-H launch vehicle was accomplished in the following manner.

Stage 1:

Orbital Altitude = 110 km

$$v = \sqrt{\frac{m_e}{al}} = \sqrt{\frac{3.986(10)^5 km^3/s^2}{6378km + 110km}} = 7.838km/s$$

Stage 2:

Vehicle mass (m_i) = 41,533 kg
Burn time (tb) = 1,094 s (For GTO)
Thrust (F) = 110,000 N
Specific impulse (I_{sp}) = 462.4 s

Exhaust velocity:

$$v_e = I_{sp} g_o = 462.4s(9.81m/s^2) = 4{,}536.144m/s$$

Mass flow rate:

$$\dot{m} = \frac{F}{v_e} = \frac{110{,}000N}{4{,}536.144m/s} = 24.2496kg/s$$

Mass of propellant used:

$$m_p = \dot{m}(tb) = 24.2496kg/s(1{,}094s) = 26{,}529.14kg$$

Final vehicle mass:

$$m_f = m_i - m_p = 41{,}533kg - 26{,}529.14kg = 15{,}003.86kg$$

Mission velocity change:

$$\Delta v = -v_e \ln(\frac{m_f}{m_i}) = -4{,}536.144m/s \ln(\frac{15{,}003.86kg}{41{,}533kg}) = 4{,}618.61m/s$$

Maximum velocity change possible:

$$\Delta v = -v_e \ln(\frac{m_f}{m_i}) = -4{,}536.144m/s \ln(\frac{14{,}333kg}{41{,}533kg}) = 4{,}826.11m/s$$

An example of the velocity change (Δv) effect on required propellant and burn time is shown in the Tables 24, 25, and 26. Single CERMET, PBR (19-Element), or TIC (19-Element) used without shielding.

Table 24. Increases in 2nd Stage Δv with a CERMET Reactor (No Shielding)

Δv (m/s)	m_{extra} (kg)	Burn Time (s)
2,000	18,138	676
3,000	14,601	961
4,000	11,442	1,215
4,619	9,658	1,359
5,000	8,620	1,443
6,000	6,099	1,646
7,000	3,847	1,827
8,000	1,836	1,989
9,000	39	2,134

Table 25. Increases in 2nd Stage Δv with a PBR (No Shielding)

Δv (m/s)	m_{extra} (kg)	Burn Time (s)
2,000	19,113	686
3,000	15,918	981
4,000	13,021	1,249
4,619	11,366	1,401
5,000	10,396	1,491
6,000	8,017	1,711
7,000	5,861	1,911
8,000	3,907	2,091
9,000	2,136	2,255
10,300	78	2,445

Table 26. Increases in 2nd Stage Δv with a TIC at 2,400-K (No Shielding)

Δv (m/s)	m_{extra} (kg)	Burn Time (s)
2000	17,952	674
3000	14,352	957
4000	11,145	1,209
4619	9,340	1,351
5000	8,289	1,434
6000	5,745	1,634
7000	3,479	1,812
8000	1,460	1,970
8800	5	2,085

Appendix G

In sizing the PBR, a choice between 3 configurations known to satisfy core criticality requirements and fit together in a near circular configuration will result in different core volumes and masses. The designer can choose amongst these configurations based on the space available for the reactor or based on the limiting the mass of the rocket as much as possible. The core will the smallest radius will result in the smallest shadow shield areas and subsequently the lightest shadow shield, but the core with the smallest radius is not always the lightest. The values that were set in this analysis are the dimension of the pellets and the percentage of the core volume that is occupied by the pellets and moderator material. Table 27 displays these values.

Table 27. PBR Set Values

Pellet Outer Diameter (mm)	Pellet Inner Diameter (mm)	Total Pellet Volume (m^3)	Volume of Inner Material (m^3)	Coating Mass (kg)	Percent Pellet	Percent Moderator
500	300	$6.545(10)^{-11}$	$1.4137(10)^{-11}$	$3.453(10)^{-7}$	8%	58%

For the cases of 18% and 33% of the power generated being lost to radiation the core dimensions are calculated and shown in Table 28 below. The estimate of core weight will change for a TIC design based on the replacement of the inner pellet material and moderator material with various materials that are beneficial to the core's ability to absorb gamma-radiation and possibly produce trigger photons of the desired energy. The masses calculated here assume all of the pellets and moderator material are constructed of the metals listed. In actuality, the pellets and moderator could be a mix of different materials, and the moderator dimensions could be reduced since there is no longer a need to moderate neutrons within the core.

Table 28. 2nd Stage PBR Reactor Sizing Analysis

Configuration	7 Element		19 Element		37 Element	
Percent of Power Radiated	18%	33%	18%	33%	18%	33%
Core Radius (m)	0.3119	0.3562	0.3558	0.3438	0.8078	0.5834
Core Height (m)	2.187	2.4196	0.8076	0.9215	0.4239	0.4742
Core Volume (m^3)	0.6691	0.9111	0.3212	0.3421	0.7228	0.5071
Core Mass (kg)	1,071	1,458	514	547	1,157	811
Lead Shadow-Shield Mass (kg)	421	574	548	537	2,823	1,540
Power Density (GW/m^3)	0.769	0.695	1.602	1.850	0.712	1.248
Pellet Volume Occupied (m^3)	0.0535	0.0729	0.0257	0.0274	0.0578	0.0406
Coating Mass (kg)	282	385	136	144	305	214
Hf Pellet Mass (kg)	154	210	74	79	166	117
W Pellet Mass (kg)	218	296	104	111	235	165
Ta Pellet Mass (kg)	193	262	92	98	208	146
Re Pellet Mass (kg)	243	331	117	124	263	184
Os Pellet Mass (kg)	260	354	125	133	281	197
Hf Moderator Mass (kg)	5,165	7,034	2,480	2,641	5,580	3,915
W Moderator Mass (kg)	7,304	9,945	3,506	3,734	7,890	5,535
Ta Moderator Mass (kg)	6,461	8,798	3,102	3,304	6,980	4,897
Re Moderator Mass (kg)	8,157	11,108	3,916	4,171	8,812	6,182
Os Moderator Mass (kg)	8,732	11,890	4,192	4,464	9,433	6,618

Appendix H

H.1 Thermal Efficiency of Fission Designs

The nuclear fission core thermal efficiency values displayed in Table 8 are calculated in the fashion shown below.

Thermal Efficiency Calculation (Fission PBR):

Tabulated values: Power = 1,945 MW, F = 333,617 N, T = 3,200 K, e = 125:1
Calculated Power = 1,598 MW
Thermal Efficiency = 1,598/1,945 = 82% $Eff = \frac{P_{core}}{P_{tabulated}}$

Thermal Efficiency Calculation (Fission CERMET):

Tabulated values: Power = 2,000 MW, F = 445,267 N, T = 2,507 K, e = 120:1
Calculated Power = 1,798 MW
Thermal Efficiency = 1,798/2,000 = 90%

Thermal Efficiency Calculation (Fission NERVA):

Tabulated values: Power = 1,570 MW, F = 334,061 N, T = 2,361 K, e = 100:1
Calculated Power = 1,299 MW
Thermal Efficiency = 1,299/1,570 = 83%

H.2 PBR Fission Design

An example of the analysis of a PBR operating on the principals of nuclear fission is carried out below.

H.2.1 Rocket Nozzle Analysis

Inputs
Mission: 2nd stage of Delta IV-H rocket
Propellant: H_2 (molecular mass 2.016 kg/kmol)
Propellant temperature (T_{o2}): 3,200 K
Chamber pressure (P_{o2}): 6,176,000 Pa
Nozzle expansion ratio (e): 285:1
Thrust (F): 110,000 N

Specific heat of hydrogen at 3,200 K:

$$c_{p_{H_2}} = \frac{1{,}000\,J/kJ}{2.016 kg/kmol}[56.505 - 702.74(\frac{3{,}200}{100})^{-0.75} + 1{,}165(\frac{3{,}200}{100})^{-1} - 560.7(\frac{3{,}200}{100})^{-1.5}]kJ/kmol-K = 18{,}642(J/kg-K)$$

Ratio of specific heats:

$$g = \frac{c_p}{c_p - \frac{R}{MM_{H_2}}} = \frac{18{,}642(J/kg-K)}{18{,}642(J/kg-K) - \frac{8{,}314.51(J/kmol-K)}{2.016(kg/kmol)}} = 1.284$$

Acoustic velocity at stagnation temperature:

$$a_o = \sqrt{g\frac{R}{MM_{H_2}}T_o} = \sqrt{1.284(\frac{8{,}314.15 J/kmol-K}{2.016 kg/kmol})3200K} = 4116.6 m/s$$

Characteristic velocity:

$$c^* = \frac{a_o}{g(\frac{2}{g+1})^{\frac{g+1}{2g-2}}} = \frac{4116.6 m/s}{1.284(\frac{2}{1.284+1})^{\frac{1.284+1}{2(1.284)-2}}} = 5468.4 m/s$$

Iteratively solve for Mach number at the nozzle exit:

$$0 = M_3(285) - [(\frac{2}{1.284+1})(1+\frac{1.284-1}{2M_3^{\,2}})]^{\frac{1.284+1}{2(1.284)-2}} \rightarrow \mathrm{M_3} = 6.7625$$

Ratio of exit pressure to chamber pressure (also referred to as stagnation pressure)

$$\frac{P_e}{P_{o2}} = \left[1+\frac{g-1}{3}M_3^2\right]^{\frac{g}{1-g}} = \left[1+\frac{(1.284-1)}{2}(6.7625)^2\right]^{\frac{1.284}{1-1.284}} = 1.11(10)^{-4}$$

Specific impulse:

$$I_{sp} = \frac{5{,}468.4 m/s(1.284)}{9.81 m/s^2}\left[(\frac{2}{1.284-1})(\frac{2}{1.284+1})^{\frac{1.284+1}{1.284-1}}\{1-(1.11(10)^{-4})^{\frac{1.284-1}{1.284}}\}\right]^{0.5} = 1036.6s$$

Exhaust velocity:

$$v_e = I_{sp}g_o = 1036.6s(9.81 m/s^2) = 10{,}169.046 m/s$$

Mass flow rate:

$$\dot{m} = \frac{F}{I_{sp}g_o} = \frac{110{,}000N}{1036.6s(9.81 m/s^2)} = 10.817 kg/s$$

Power needed to heat propellant to desired temperature:

$$P_{core} = \frac{1000 J/kJ(10.817 kg/s)}{2.016 kg/kmol}[0 + 56.505(3200-300) - \frac{702.74(100)^{0.75}}{0.25}(3200^{0.25} - 300^{0.25})$$

$$+ 1{,}165(100)(\ln(3200) - \ln(300)) - \frac{560.7(100)^{1.5}}{-0.5}(3200^{-0.5} - 300^{-0.5})]kJ/kmol-K = 516 MW$$

Core radius:

$$R_{core} = -2.655(10)^{-12}(\frac{516}{0.82})^5 + 8.946(10)^{-9}(\frac{516}{0.82})^4 - 1.1703(10)^{-5}(\frac{516}{0.82})^3$$
$$+ 7.427(10)^{-3}(\frac{516}{0.82})^2 - 2.2955(\frac{516}{0.82}) + 313.34 = 34.43cm$$

Core height:

$$H_{core} = -4.027(10)^{-5}(\frac{516}{0.82})^2 + 0.1427(\frac{516}{0.82}) + 17.9883 = 91.84cm$$

Core volume:

$$V_{core} = pR_{core}^2 H_{core} = p(.3443m)^2(.9184m) = 0.3420m^3$$

Core mass:

$$m_{core} = r_{core} V_{core} = (1{,}600kg/m^3).3420m^3 = 547kg$$

Shadow mass: (S_l is shield loading which is 3,500 kg/m^2 for a fission shield)

$$m_{shield} = S_l A_{shield} = S_l pR_{core}^2 = 3{,}500kg/m^2 p(.3443m)^2 = 1{,}303.44kg$$

H.2.2 Mission Details

Δv Requirement: 4,618.61 m/s
Initial Mass (m_i): 41,533 kg
Propellant Mass (m_{prop}): 27,200 kg
Payload Mass (m_l): 10,800 kg
Pressure Drop through the Core (P_{drop}): 5%

Final vehicle mass:

$$m_f = m_i(e^{\frac{-\Delta v}{v_e}}) = 41{,}533kg(e^{\frac{-4{,}618.61m/s}{10{,}169.046m/s}}) = 26{,}372.06kg$$

Mass of propellant used for specified mission:

$$m_p = m_i - m_f = 41{,}533kg - 26{,}372.06kg = 15{,}160.94kg$$

Fuel savings due to high I_{sp}:

$$m_{extra} = m_{prop} - m_p = 26{,}529.14kg - 15{,}160.94kg = 11{,}368.20kg$$

Current system structural mass without chemical engine:

$$m_s = 3{,}490kg - 301kg = 3{,}189kg$$

Inert mass fraction if all savings is used for structural redesign to include fission core:

$$f_{inert} = \frac{(m_{extra} + m_s)}{m_p + (m_{extra} + m_s)} = \frac{(11{,}368.20kg + 3{,}189kg)}{15{,}160.94kg + (11{,}368.20kg + 3{,}189kg)} = 0.4898$$

Inert mass fraction if all savings is used for additional payload:

$$f_{inert} = \frac{(m_s + m_{core} + m_{shield})}{m_p + (m_s + m_{core} + m_{shield})} = \frac{(3{,}189kg + 547kg + 1{,}303.44kg)}{15{,}160.94kg + (3{,}189kg + 547kg + 1{,}303.44kg)} = 0.2495$$

Check for feasibility:

$$1 - f_{inert} e^{\frac{\Delta v}{I_{sp} g_o}} = 1 - 0.4898 e^{\frac{-4{,}618.61 m/s}{1036.6 s(9.81 m/s^2)}} = 0.6899 > 0$$

H.3 Core Breakup

300 *mm* diameter sphere → $V_{pi} = 1.4137(10)^{-11}$ m^3
500 *mm* diameter sphere → $V_{po} = 6.545(10)^{-11}$ m^3

Mass of fuel in fission PBR:

$$m_{fuel} = \frac{1}{3} M_{core} = \frac{1}{3} 547kg = 182kg$$

Mass of moderator in fission PBR

$$m_{moderator} = \frac{2}{3} M_{core} = \frac{2}{3} 547kg = 365kg$$

Mass of single pellet including coating and fuel:

$$m_{pellet} = \rho_{UC_2} V_{pi} + \rho_{ZrC}(V_{po} - V_{pi}) = 11{,}300kg/m^3 (1.4137(10)^{-11}) + 6{,}730kg/m^3$$
$$(6.545(10)^{-11} - 1.4137(10)^{-11}) = 5.0508(10)^{-7} kg$$

Number of pellets within fission PBR:

$$N_p = \frac{m_{fuel}}{m_{pellet}} = \frac{182kg}{5.0508(10)^{-7} kg} = 360{,}335{,}682$$

Volume occupied by pellets in fission PBR:

$$V_p = \frac{N_p V_{po}}{0.88} = \frac{360{,}335{,}682(6.545(10)^{-11})}{0.88} = 0.0268m^3$$

Volume occupied by moderator in fission PBR:

$$V_{\text{mod}} = \frac{m_{\text{mod}}}{r_{Be}} = \frac{365kg}{1{,}848kg/m^3} = 0.1975m^3$$

Percent of core that is pellets by volume

$$P_{bvp} = \frac{V_p}{V_{core}} = \frac{0.0268m^3}{0.3420m^3} = 0.0784 \approx 8\%$$

Percent of core that is moderator by volume

$$P_{bvm} = \frac{V_{\text{mod}}}{V_{core}} = \frac{0.1975m^3}{0.3420m^3} = 0.5775 \approx 58\%$$

H.4 TIC Mass Changes

2nd Stage Mission
For 514.63 MW (82% efficiency)
Core sized at V_{core} = 0.3212 m^3.
Percent of pellet volume that is core material equals 21.6% (300 μm diameter)
Percent of pellet volume that is coating material equals 78.4% (500 μm diameter)

Total mass of pellets within the core if all are metallic hafnium:

$$m_{Hf} = r_{Hf} P_{bvp}(0.216)V_{core} = 13{,}310kg/m^3(0.08)(0.216)(0.3212m^3) = 73.87kg$$

Total sum of all pellets coating material:

$$m_{ZrC} = r_{ZrC} P_{bvp}(0.784)V_{core} = 6{,}730kg/m^3(0.08)(0.784)(0.3212m^3) = 135.58kg$$

Mass resulting from replacing moderator with metallic hafnium:

$$m_{Hf\,\text{mod}} = r_{Hf} P_{bvm} V_{core} = 13{,}310kg/m^3(0.58)(0.3212m^3) = 2{,}479.6kg$$

H.4.1 Shielding the 19-Element TIC

R_{core} = 0.3558 m

Power radiated from the core:

$$P_{rad} = \frac{P_{core}}{0.82} - P_{core} = \frac{422(10)^6 W}{0.82} - 422(10)^6 W = 92.63(10)^6 W$$

Mass energy-absorption coefficient (m_A / r = 0.0027 m^2/kg) is an average value for air (40:369)
Range (r = 3 m) from source to sensitive components.

Allowable dose rate ($\dot{D}$ = 0.01 rad/s)

Dose rate without shielding:

$$\dot{D}_o = \frac{P_{rad}}{4pr^2}\frac{m_A}{r} = \frac{92.63(10)^6 W}{4p(3m)^2}(0.0027m^2/kg) = 2{,}211.378J/kg = 221{,}137.84rad/s$$

Relaxation length:

$$mx = -\log(\frac{\dot{D}}{\dot{D}_o B})$$

Using Fig. 7, the Buildup Factor (B) was found to be 2.7 with a relaxation length of 17.9.

Lead shield thickness:

$$x = \frac{mx}{m_{Pb}} = \frac{17.9}{148.2} = 0.1208m$$

Shield loading:

$$S_l = r_{Pb}x = 11{,}400kg/m^3(.1208m) = 1{,}377.12kg/m^2$$

Shadow shield mass:

$$m_{shield} = A_{shield}S_l = pR_{core}^2 S_l = p(0.3558m)^2(1{,}377.12kg/m^2) = 547.69kg$$

H.4.2 Maximum Pellet Temperature for TIC

Thermal conductivity (k = 1.9 W/m-K)
Maximum static temperature of propellant flow (T_2 = 2,400 K)
Thickness of zirconium carbide coating (x = 100 mm)
Outer diameter of pellet (d_o = 500 mm)
Power needed to heat H2 to 2,400 K (P_{core}= 422 MW)
The mass of hafnium (m_{Hf}) pellets in the core is determined from the core size in beginning of H.4.

Surface area of pellet:

$$A = 4p(\frac{d_o}{2})^2 = 4p(\frac{500(10)^{-6}m}{2})^2 = 7.854(10)^{-7}m$$

Mass of single hafnium pellet without the coating:

$$m_{Hfs} = V_{pi}r_{Hf} = 1.4137(10)^{-11}m^3(13{,}310kg/m^3) = 1.882(10)^{-7}kg$$

Number of hafnium pellets in the core: (very sensitive to rounding)

$$N_p = \frac{m_{Hf}}{m_{Hfs}} = \frac{73.87kg}{1.882(10)^{-7}kg} = 392{,}610{,}592$$

Power absorbed and available per pellet for propellant heating (if evenly distributed!):

$$\dot{Q}_x = \frac{P_{core}}{N_p} = \frac{422(10)^6 W}{392{,}610{,}592} = 1.075W$$

Pellet interior temperature:

$$T_p = T_2 + \frac{\dot{Q}_x \Delta x}{kA} = 2{,}400K + \frac{1.075W(100(10)^{-6} m)}{1.9W/m - K(7.854(10)^{-7} m)} = 2{,}472K$$

The thermal conductivity is varied to determine the affect on the required fuel surface temperature for heating. The values are calculated using Eq. [44] and graphed in Fig. 10.

Table 29. Generic Case: Variation of Temperature with Thermal Conductivity.

Thermal Conductivity (W/m-K)	**Fuel Surface Temperature (K)**
0.2	3084
0.5	2674
1	2537
1.9	2472
3	2446
4	2434
100	2401

H.5 Sizing a NERVA Fission Core

Typical NERVA power density (P_{den} = 1.57 GW/m^3)
Typical NERVA density (r_{NERVA} = 2,300 kg/m^3)
Required power for 2nd Stage mission (P_{core} = 417 MW)
Core efficiency = 83%

Required core power:

$$P_{req} = \frac{P_{core}}{0.83} = \frac{417(10)^6 W}{0.83} = 502.4MW$$

Radiated power:

$$P_{rad} = P_{req} - P_{core} = 502.4MW - 417MW = 85.4MW$$

Core volume:

$$V_{core} = \frac{P_{req}}{P_{den}} = \frac{502.4(10)^6 W}{1.57(10)^9 W/m^3} = 0.3200m^3$$

Approximate $H_{core} = 2R_{core}$

Core Radius:

$$R_{core} = \sqrt[3]{\frac{V_{core}}{2p}} = \sqrt[3]{\frac{0.3200m^3}{2p}} = 0.3707m$$

Core Height:

$$H_{core} = 2R_{core} = 2(0.3707m) = 0.7413m$$

Core Mass:

$$m_{core} = r_{NERVA} V_{core} = 2{,}300kg/m^3(0.3200m^3) = 736kg$$

Shadow mass: (S_l is shield loading which is 3,500 kg/m^2 for a fission shield)

$$m_{shield} = S_l A_{shield} = S_l p R_{core}^2 = 3{,}500kg/m^2 p(.3707m)^2 = 1{,}511kg$$

H.6 Sizing a CERMET Fission Core

Typical CERMET density (r_{CERMET} = 8,500 kg/m^3)
Required power for Stage II mission (P_{core} = 435 MW)
Core efficiency = 90%

Required core power:

$$P_{req} = \frac{P_{core}}{0.90} = \frac{435(10)^6 W}{0.90} = 483.3MW$$

Radiated power:

$$P_{rad} = P_{req} - P_{core} = 483.3MW - 435MW = 48.3MW$$

Core radius:

$$R_{core} = 0.0034P_{req} + 20.79 = 0.0034(483.3) + 20.79 = 22.43cm = 0.2243m$$

Core height:

$$H_{core} = 0.0067 P_{req} + 41.418 = 0.0067(483.3) + 41.418 = 44.66 cm = 0.4466 m$$

Core volume:

$$V_{core} = p\, R_{core}^2 H_{core} = p\, (0.2243 m)^2 (0.4466\, m) = 0.0706 m^3$$

Core mass:

$$m_{core} = r_{CERMET} V_{core} = 8{,}500 kg / m^3 (0.0706 m^3) = 600.1 kg$$

Shadow mass: (S_l is shield loading which is 3,500 kg/m^2 for a fission shield)

$$m_{shield} = S_l A_{shield} = S_l p\, R_{core}^2 = 3{,}500 kg / m^2 p\, (0.2243 m)^2 = 553.2 kg$$

Appendix I

Outlined here is the process for estimating the core efficiency of a gamma producing source. As noted in the paper, a spherical layer of material is placed around a point source generating only gamma photons of 500 keV.

Source power = 600 MW
Radius to outer surface of core $R = 0.3\text{m} = 30$ cm
Linear attenuation coefficient for lead $m = 1.83$ cm^{-1}
Linear absorption coefficient for lead $m_A = 1.035$ cm^{-1}
Linear attenuation coefficient for tungsten $m = 2.66$ cm^{-1}
Linear absorption coefficient for tungsten $m_A = 1.44$ cm^{-1}

Source strength:

$$S = 600(10)^6 J/s(6.2415(10)^{18} eV/J)(\frac{1}{500(10)^3 eV/photon}) = 7.5(10)^{21} photons/s$$

Uncollided photon flux:

$$\Gamma^o(30,x) = \frac{Se^{-mx}}{4pR^2} = \frac{7.5(10)^{21} photons/s(e^{-mx})}{4p(30cm)^2} = 6.63(10)^{17} e^{-mx} photons/cm^3 - s$$

For the case of $mx = 4$

$$\Gamma^o(30,2.186) = \frac{7.5(10)^{21} photons/s(e^{-4})}{4p(30cm)^2} = 1.215(10)^{16} photons/cm^3 - s$$

Rate of heat deposition at materials outer surface per unit volume:

$$H(30,2.186) = 1.062(10)^{-6} erg/MeV(10^{-7} J/erg) m_a E_o B_a(mx)\Gamma^o(30,2.186)$$
$$= 1.062(10)^{-13} J/MeV(1.035cm^{-1})(0.5MeV)(2.19)1.215(10)^{16} photon/cm^3 - s$$
$$= 1462.36W/cm^3$$

Volume of material:

$$V = \frac{4}{3}p[(R+x)^3 - R^3] = \frac{4}{3}p[(30cm + 2.186cm)^3 - (30cm)^3] = 26{,}568cm^3$$

Rate of heat deposition:

$$H_{final}(R,x) = H(R,x)V = 1462.36W/cm^3(26{,}568cm^3) = 38851980W = 38.9MW$$

Mass of material:

$$m = r_{Pb}V = 11.34g/cm^3(26{,}568cm^3) = 301{,}281g = 301kg$$

Core efficiency:

$$Eff = 1 - \frac{P_{radiated}}{P_{produced}} = 1 - \frac{38.9MW}{600MW} = 93\%$$

Values for the two materials are tabulated as follows.

Table 30. Spherical Shell Values for Lead

mx	x (cm)	B_a	$\Gamma^o(R,x)$ (photons/cm^3-s)	$H(R,x)$ (W/cm^3)	V (cm^3)	H (MW)	m (kg)
1	0.546	1.51	$2.4396(10)^{17}$	20,246	6,288	127.3	71.3
2	1.093	1.80	$8.975(10)^{16}$	8,879	12,817	113.8	145
4	2.186	2.19	$1.215(10)^{16}$	1,462	26,568	38.9	301
7	3.825	2.61	$6.047(10)^{14}$	87	49,009	4.3	556
10	5.464	3.01	$3.011(10)^{13}$	5	73,735	0.4	836
15	8.197	3.52	$2.028(10)^{11}$	0.04	120,343	0.005	1,365

Table 31. Spherical Shell Values for Tungsten

mx	x (cm)	B_a	$\Gamma^o(R,x)$ (photons/cm^3-s)	$H(R,x)$ (W/cm^3)	V (cm^3)	H (MW)	m (kg)
1	0.376	1.64	$2.4396(10)^{17}$	30,585	4,306	131.7	83
2	0.752	2.16	$8.975(10)^{16}$	14,862	8,720	129.6	168
4	1.50	3.26	$1.215(10)^{16}$	3,029	17,827	54	344
7	2.63	5.43	$6.047(10)^{14}$	251	34,428	8.64	664
10	3.76	8.37	$3.011(10)^{13}$	19	48,077	0.93	927
15	5.64	15.17	$2.028(10)^{11}$	0.235	76,530	0.018	1,477

Due to the rough nature of this estimation the core efficiencies generated for the nuclear fission cores were used in the analysis. These numbers were merely generated to provide

a level of confidence that high efficiencies with mass quantities of materials, not prohibitive to a TIC design, are possible for heating due gamma-ray emission. The efficiencies across the range of thicknesses used are shown in Table 32.

Table 32. Spherical Core Efficiencies

Material	Lead		Tungsten	
mx	x (cm)	Eff	x (cm)	Eff
1	0.546	78.8%	0.376	78%
2	1.093	81%	0.752	78.4%
4	2.186	93.5%	1.50	91%
7	3.825	99.3%	2.63	98.6%
10	5.464	99.9%	3.76	99.8%
15	8.197	99.99%	5.64	99.99%

Bibliography

1. Zubrin, Robert. *Entering Space; Creating a Spacefaring Civilization.* New York: Penguin Putnam Inc., 1999.

2. Hamilton, Christopher E. *Design Study of Triggered Isomer Heat Exchanger-Combustion Hybrid Jet Engine for High Altitude Flight.* MS thesis, AFIT/GAE/ENY/02-6. School and Engineering and Management, Air Force Institute of Technology (AU), Wright-Patterson AFB OH, March 2002 (ADA401290).

3. Humble, R.W., G.N. Henry, and W.J. Larson. *Space Propulsion Analysis and Design.* New York: McGraw-Hill Companies, 1995.

4. Cinnamon, John D. "Nuclear Thermal Rocket Propulsion Design Issues and Concepts." Department of Aerospace Engineering, University of Texas at Austin. 20 February 2004. http://www.tsgc.utexas.edu/archive/fulltext/nuke.pdf

5. Federation of American Scientists. "Nuclear Rocket Propulsion – The 60s." 20 February 2004. http://www.fas.org/nuke/space/c04rover.htm

6. Federation of American Scientists. "SDI – Nuclear and Other Power Sources." 20 February 2004. http://www.fas.org/nuke/space/c06sdi_2.htm

7. Space Daily. "NASA Contracts for $6 Million Nuclear Electric Propulsion Study." 20 February 2004. http://www.spacedaily.com/news/nuclearspace-03m.html

8. Office of the Press Secretary. "President Bush Announces New Vision for Space Exploration Program." 20 February 2004. http://www.whitehouse.gov/news/releases/2004/01/20040114-1.html

9. Collins, C.B, F. Davanloo, M.C. Iosif, R. Dussart, J.M. Hicks, S.A. Karamian, C.A. Ur, I.I. Popescu, V.I. Kirischuk, J.J. Carroll, H.E. Roberts, P. McDaniel, and C.E. Crist. "Accelerated Emission of Gamma Rays from the 31-yr Isomer ^{178}Hf Induced by X-Ray Irradiation." *Physical Review Letters,* 82: 695-698 (January 1999).

10. Collins, C.B. *Research on Intense Pulsed Power for Electromagnetic Radiation: Final Technical Report, 1 January 1999-30 November 2001.* Grant F49620-99-1-0082. Richardson TX: Center for Quantum Electronics, December 2001 (ADA397697).

11. Etherington, Harold E. *Nuclear Engineering Handbook.* New York: McGraw-Hill Book Company, Inc., 1958

12. Ahmad, I., J.C. Banar, J.A. Becker, T.A. Bredeweg, J.R. Cooper, D.S. Gemmell, A. Mashayekhi, D.P. McNabb, E.F. Moore, P. Palmer, R.S. Rundberg, J.P. Schiffer, S.D. Shastri, T.F. Wang, and J.B. Wilhelmy. "Search for x-ray induced decay of the 31-yr isomer of ^{178}Hf at low x-ray energies. *Physical Review Letters,* 67: 041305 (April 2003).

13. Ahmad, I., J.C. Banar, J.A. Becker, D.S. Gemmell, A. Kraemer, A. Mashayekhi, D.P. McNabb, G.G. Miller, E.F. Moore, L.N. Pangault, R.S. Rundberg, J.P. Schiffer, S.D. Shastri, T.F. Wang, and J.B. Wilhelmy. "Search for X-Ray Induced Acceleration of the Decay of the 31-Yr Isomer of 178Hf Using Synchrotron Radiation." *Physical Review Letter,* 87: 072503 (July 2001).

14. Stark, Anne. "Physicists challenge reports of accelerated decay of nuclear excited states." *Lawrence Livermore National Laboratory Public Release,* 13 August 2001.

15. Olariu, Silviu and Agata Olariu. "Comment on 'Accelerated Emission of Gamma Rays from the 31-yr Isomer of ^{178}Hf Induced by X-ray Irradiation.'" *Physical Review Letters,* 84: 2541 (March 2000).

16. McNabb, D.P., J.D. Anderson, J.A. Becker. "Comment on 'Accelerated Emission of Gamma Rays from the 31-yr Isomer of ^{178}Hf Induced by X-ray Irradiation.'" *Physical Review Letters,* 84: 2542 (March 2000).

17. Ahmad, I., J.C. Banar, J.A. Becker, D.S. Gemmell, A. Kraemer, A. Mashayekhi, D.P. McNabb, G.G. Miller, E.F. Moore, L.N. Pangault, R.S. Rundberg, J.P. Schiffer, S.D. Shastri, T.-F. Wang, and J.B. Wilhelmy. "Search for X-Ray Induced Acceleration of the Decay of the 31-Yr Isomer of ^{178}Hf Using Synchrotron Radiation." *Physical Review Letters,* 87: 072503 (2001).

18. Advanced Propulsion Technology Group. "Advanced Propulsion Concepts." Internet Article, Jet Propulsion Laboratory, Pasadena CA. 20 February 2004. http://www.islandone.org/APC/Introduction/06.html

19. Taiwo, T.A., M. Fatone, G. Palmiotti, and R.N. Hill. "Physics Studies for a Particle-Bed Gas Cooled Fast Reactor Core Design." 20 February 2004. http://www.iaea.or.at/inis/aws/htgr/fulltext/htr2002_305.pdf

20. Federation of American Scientists. "Timberwind." 20 February 2004. http://www.fas.org/nuke/space/c08tw_2.htm

21. Federation of American Scientists. "TW/SNTP." 20 February 2004. http://www.fas.org/nuke/space/c08tw_1.htm

22. Isakowitz, S.J., J.P. Hopkins Jr., J.B. Hopkins. *International Reference Guide to Space Launch Systems (3rd Edition).* Virginia: American Institute of Aeronautics and Astronautics, Inc., 1999.

23. Hartsfield, Carl R. *Analysis of the Application of a Triggered Isomer Heat Exchanger as a Replacement for the Combustion Chamber in an Off-The-Shelf Turbojet.* MS thesis, AFIT/GAE/ENY/01M-04. School and Engineering and Management, Air Force Institute of Technology (AU), Wright-Patterson AFB OH, March 2002 (ADA390148).

24. ANSYS, Inc. *ANSYS Multiphysics.* Finite Element Software Version 5.6.1. Southpointe, Canonsburg, PA (1-800-937-3321), 1999.

25. McDaniel, Patrick. Department Manager for High Power Electromagnetic Systems, Department 15331, Sandia National Laboratories, Albuquerque NM. Personal Correspondence. 18 April 2003.

26. Mattingly, Jack. AEDSYS: Aircraft Engine Design System Analysis Software (Version 2.13 – December 14, 2001 for Windows 95/98/NT). http://www.aircraftenginedesign.com, with permission of author.

27. Mattingly, Jack. ONX: Parametric Cycle Analysis – On Design Analysis of Gas Turbine Engines (Version 4.021 – December 18, 2001 for Windows 95/98/NT). http://www.aircraftenginedesign.com, with permission of author.

28. Collins, C.B, A.C. Rusu, N.C. Zoita, M.C. Iosif, D.T. Camase, F. Davanloo, C.A. UR, I.I. Popescu, J.M. Pouvesle, R. Dussart, V.I. Kirischuk, N.V. Strilchuk, and F.J. Agee. "Gamma-Ray Transitions Induced in Nuclear Spin Isomers by X-Rays." *Hyperfine Interactions,* 135: 51-70 (2001).

29. Collins, C.B, F. Davanloo, M.C. Iosif, R. Dussart, J.M. Hicks, S.A. Karamian, C.A. Ur, I.I. Popescu, V.I. Kirischuk, H.E. Roberts, P. McDaniel, and C.E. Crist. "Collins et al. Reply." *Physical Review Letters,* 84: 2544-2545 (March 2000).

30. Agee, Forrest J. "Review of Induced Gamma Emission and Gamma-Ray Laser Research." *Hyperfine Interactions,* 143:1-6 (2002).

31. Walker, P.M. and G.D. Dracoulis. "Exotic Isomers in Deformed Atomic Nuclei." *Hyperfine Interaction,* 135: 83-107 (January 2001).

32. Hambling, David. "Gamma-ray weapons could trigger next arms race." 20 February 2004. http://www.newscientist.com/news/news.jsp?id=ns99994049

33. Belov, A.G., Yu.P. Gangrsky, A.P. Tonchev, and P. Zuzaan. "Excitation of the high-spin ^{180}Hf isomer and de-excitation of the ^{180}Ta isomer in (g ,g ') reactions." *Hyperfine Interactions,* 107: 167-173 (January 1997).

34. McDaniel, Patrick. Department Manager for High Power Electromagnetic Systems, Department 15331, Sandia National Laboratories, Albuquerque NM. Personal Communication, 23 January 2004.

35. Agee, Forrest J. Director of Physics and Electronics, Air Force Office of Scientific Research, Electronic Message. 5 December 2003.

36. Lamarsh, John R., and A.J. Baratta. *Introduction to Nuclear Engineering (3rd Edition)*. New Jersey: Prentice-Hall, Inc., 2001.

37. Space War. "Can Robots Fly on Nuke Power Alone?" 20 February 2004. http://www.spacewar.com/news/uav-03m.html

38. Carson, M., R. Diz, S. Long, K. MacArthur, K. Totty. "Radiation Hardening of Electronics." MSE 4206 Class Presentation, Virginia Tech, VA. 20 February 2004. http://www.mse.vt.edu/faculty/hendricks/mse4206/projects97/group02/radhard.htm

39. Callister, William D. *Materials Science and Engineering an Introduction*, 3rd edition. New York: John Wiley & Sons, Inc., 1994.

40. Turner, James E. *Atoms, Radiation, and Radiation Protection (2nd Edition)*. New York: John Wily & Sons, Inc., 1995.

41. Monier, Eric. "Radio to Gamma Rays." 20 February 2004. http://www-astronomy.mps.ohio-state.edu/~monier/Ast161/Unit3/radiogamma.html

42. "Space Fission Reactor Power Systems. Their Use and Safety." *NASA*. 20 February 2004. http://spacescience.nasa.gov/missions/fissiontechsafety.pdf

43. Dooling, Dave. "Nuclear Power: The Future of Spaceflight?" 20 February 2004. http://www.space.com/businesstechnology/nuclear_power_000718.html

44. NASA. "Great Images in NASA; NASA Summary of historical testing." 20 February 2004. http://grin.hq.nasa.gov/ABSTRACTS/GPN-2002-000143.html

45. Mars Academy. "Nuclear Engines." 20 February 2004. http://www.marsacademy.com/propul/propul6.htm

46. Willaume, R.A., A. Jaumotte, R.W. Bussard. *Nuclear, Thermal and Electric Rocket Propulsion.* New York: Gordon and Breach, Science Publishers Inc., 1967.

47. Curran, H. J., Gaffuri, P., Pitz, W. J., and Westbrook, C. K. "A Comprehensive Modeling Study of iso-Octane Oxidation" *Combustion and Flame* 129:253-280 (2002). 20 February 2004. http://www-cms.llnl.gov/combustion/combustion2.html#i-C8H18

48. Saad, Michel A. *Compressible Fluid Flow, 2nd Edition.* New Jersey: Prentice Hall, Inc., 1993.

49. X-Ray Transition Energies Database, Online. *National Institute of Standards and Technologies.* 20 February 2004. http://www.nist.gov/srd/atomic.htm

50. Chemical Fact Sheets. 20 February 2004. http://www.speclab.com

51. Beck, Dan. "RS-68 Engine." 20 February 2004. http://www.boeing.com/defense-space/space/propul/RS68.html

52. Space and Tech Rocket Engine Database. http://www.spaceandtech.com/spacedata/engines/rl10_specs.shtml

53. Sarner, Stanley F. *Propellant Chemistry.* New York: Reinhold Publishing Co., 1966.

54. WebElements™ Periodic Table. 20 February 2004. http://www.webelements.com

55. Barbalace, K.L. "Periodic Table of Elements Sorted by Thermal Conductivity." 20 February 2004. http://www.environmentalchemistry.com/yogi/periodic/thermal.html

56. Matweb. "Material Property Data." 20 February 2004. http://www.matweb.com/index.asp?ckck=1

57. Hubbell, J.H. and S.M. Seltzer. "Tables of X-Ray Mass Attenuation Coefficients and Mass Energy-Absorption Coefficients." National Institute of Standards and Technology. 20 February 2004. http://physics.nist.gov/PhysRefData/XrayMassCoef/cover.html

Vita

Captain Benjamin L. Johnson graduated from Washington Park High School in Racine, WI. He entered undergraduate studies at the University of Notre Dame in South Bend, Indiana where he graduated with a Bachelor of Science degree in Mechanical Engineering in May 1999. He was commissioned through the Detachment 225 AFROTC at the University of Notre Dame.

His first assignment was at Eglin AFB, Florida as an ordnance integration engineer. In August 2002, he entered the Graduate School of Engineering and Management, Air Force Institute of Technology. Upon graduation, he will be assigned to the Kirtland AFB, New Mexico.

REPORT DOCUMENTATION PAGE

Form Approved
OMB No. 074-0188

PLEASE DO NOT RETURN YOUR FORM TO THE ABOVE ADDRESS.

1. REPORT DATE *(DD-MM-YYYY)*	2. REPORT TYPE	3. DATES COVERED *(From – To)*
03-12-2004	**Master's Thesis**	Sep 2002 – Mar 2004

4. TITLE AND SUBTITLE

ISOMER ENERGY SOURCE FOR SPACE PROPULSION SYSTEMS

5a. CONTRACT NUMBER

5b. GRANT NUMBER

5c. PROGRAM ELEMENT NUMBER

6. AUTHOR(S)

Johnson, Benjamin, L., Captain, USAF

5d. PROJECT NUMBER

5e. TASK NUMBER

5f. WORK UNIT NUMBER

7. PERFORMING ORGANIZATION NAMES(S) AND ADDRESS(S)

Air Force Institute of Technology
Graduate School of Engineering and Management (AFIT/EN)
2950 Hobson Way
WPAFB OH 45433-7765

8. PERFORMING ORGANIZATION REPORT NUMBER

AFIT/GA/ENY/04-M01

9. SPONSORING/MONITORING AGENCY NAME(S) AND ADDRESS(ES)

AFRL/PRAS
Attn: Lt Jack P. Barnett
1950 Fifth St. Bldg. 18
WPAFB OH 45433-7765
DSN: 785-0303
e-mail: Jack.Barnett@wpafb.af.mil

10. SPONSOR/MONITOR'S ACRONYM(S)

11. SPONSOR/MONITOR'S REPORT NUMBER(S)

12. DISTRIBUTION/AVAILABILITY STATEMENT

APPROVED FOR PUBLIC RELEASE; DISTRIBUTION UNLIMITED.

13. SUPPLEMENTARY NOTES

14. ABSTRACT

Presented in this work are the results of an investigation of alternative means for powering spacecraft and launch vehicles with energy sources other than chemical combustion. Nuclear thermal propulsion and the energy release of a nuclear spin isomer present potential for increased rocket performance with compact, high-energy fuel sources replacing the combustion engines of the Delta IV-H 1st and 2nd stage vehicles. Analysis of historical fission designs along with the isomer hafnium-178-m2 in a particle bed configuration was conducted. Energy storage levels of 1.3 GJ/g are possible with this material, though the successful triggering and maintenance of a chain reaction in this material are still debated topics within the scientific community. The best application for either technology is as an upper stage vehicle with the shielding requirements reduced to that of just a shadow shield between the core and the spacecrafts upper structure. The fission designs are capable of specific impulse values between 800 and 1,000 s leading to mass savings in the range of 7,000 to nearly 10,000 kg once the engine masses and shielding have been included. An isomer core in the configuration of a 19-element PBR may be able to achieve a specific impulse on the order of 880 s with the isomer in metallic form, and specific impulse values as high as 1,090 s if the isomer is in the form of hafnium carbide. This translates to somewhere between a 5,000 and 9,000 kg depending on the material makeup of the core and heat efficiency. Payload mass increases by a factor of two or greater velocity changes are the payoffs of these systems.

15. SUBJECT TERMS

Triggered Isomer, Nuclear Spin Isomer, Nuclear Thermal Propulsion, Rocket Propulsion, Space Propulsion

16. SECURITY CLASSIFICATION OF:			17. LIMITATION OF ABSTRACT	18. NUMBER OF PAGES	19a. NAME OF RESPONSIBLE PERSON
a. REPORT	b. ABSTRACT	c. THIS PAGE			Milton E. Franke, PhD, USAF (ENY)
U	U	U	UU	136	19b. TELEPHONE NUMBER *(Include area code)* (937) 255-3636, ext 4720; e-mail: Milton.Franke@afit.edu

Standard Form 298 (Rev. 8-98)
Prescribed byANSI Std. Z39-18